Energy & Environmental Science

ROYAL SOCIETY OF CHEMISTRY

REVIEW

View Article Online
View Journal | View Issue

Cite this: *Energy Environ. Sci.*, 2025, **18**, 3526

Electricity-to-ammonia interconversion in protonic ceramic cells: advances, challenges and perspectives

Mingzhuang Liang,†[a] Jinwook Kim, †[b] Xiaomin Xu, [c] Hainan Sun, [d] Yufei Song,[e] SungHyun Jeon,[a] Tae Ho Shin, *[f] Zongping Shao *[c] and WooChul Jung *[ag]

NH_3 is an attractive alternative fuel to hydrogen and methane, offering advantages such as easy compression at room temperature, straightforward storage and transportation, high volumetric energy density, and carbon-free nature. However, conventional NH_3 synthesis requires high temperatures and pressures, resulting in substantial energy consumption and increased equipment and maintenance costs. Protonic ceramic cells (PCCs), as a cutting-edge energy conversion technology, can realize NH_3 synthesis at moderate pressures and low-to-intermediate temperatures by utilizing surplus renewable electricity generated by wind and solar power. Additionally, PCCs can be employed to convert NH_3 into electricity to meet instantaneous demand, providing a means to address the seasonal and intermittent nature of renewable energy sources. Despite their potential, the commercial application of electricity-to-NH_3 interconversion in PCCs faces several challenges, primarily related to insufficient performance and durability. This review systematically explores the mechanisms and challenges of electricity-to-NH_3 interconversion in PCCs, highlights recent advancements in NH_3 synthesis using PCCs and direct NH_3-fueled proton ceramic fuel cells (DA-PCFCs), and discusses perspectives for realizing high-efficiency electricity-to-NH_3 interconversion. This review aims to establish a scientific foundation for efficient electricity-to-NH_3 interconversion *via* PCCs and provides critical insights for designing high-performance and durable PCC components.

Received 22nd December 2024,
Accepted 3rd March 2025

DOI: 10.1039/d4ee06100d

rsc.li/ees

Broader context

The conventional Haber–Bosch process for NH_3 synthesis necessitates energy-intensive high-temperature and high-pressure conditions, leading to substantial energy consumption and significant operational costs. Proton ceramic cells (PCCs) offer a compelling solution by enabling the electrochemical synthesis of NH_3 from renewable electricity at intermediate temperatures and pressures. Furthermore, PCCs can efficiently convert the synthesized NH_3 back into electricity to meet instant demand, addressing the intermittency inherent in renewable energy sources. While PCCs exhibit immense potential, achieving efficient bidirectional electrochemical interconversion between electricity and NH_3 remains a critical challenge for their practical application. This review comprehensively examines the mechanisms and advantages of this electrochemical interconversion in PCCs, with a particular focus on recent advancements and critical challenges in NH_3 synthesis utilizing PCCs and direct NH_3-fueled proton ceramic fuel cells (DA-PCFCs). The review concludes with a discussion of the future prospects and critical research directions towards realizing efficient electrochemical interconversion between electricity and NH_3 using PCC technology. This review aims to establish a scientific foundation for efficient electricity-to-NH_3 interconversion *via* PCCs and provides critical insights for designing high-performance and durable PCC components.

[a] *Research Institute of Advanced Materials, Seoul National University (SNU), Seoul, 08826, Republic of Korea. E-mail: wcjung@snu.ac.kr*
[b] *Department of Materials Science and Engineering, Northwestern University, Evanston, Illinois 60208, USA*
[c] *WA School of Mines: Minerals, Energy and Chemical Engineering (WASM-MECE), Curtin University, Perth, WA 6845, Australia. E-mail: zongping.shao@curtin.edu.au*
[d] *School of Chemistry and Chemical Engineering, Nantong University, Nantong, 226019, P. R. China*
[e] *State Key Laboratory of Materials-Oriented Chemical Engineering, College of Chemical Engineering, Nanjing Tech University, Nanjing, 210009, P. R. China*
[f] *Division for Low Carbon Energy & Materials DX, Korea Institute of Ceramic Engineering and Technology (KICET), Jinju-si 52851, Republic of Korea. E-mail: ths@kicet.re.kr*
[g] *Department of Materials Science and Engineering, Seoul National University, Seoul, 08826, Republic of Korea*
† These authors contributed equally to this work.

1. Introduction

The rapid expansion of the global economy has intensified the use of traditional fossil fuels, leading to significant environmental pollution and heightened greenhouse gas emissions. To ensure environmental protection and sustainable development, there is an urgent need to identify clean energy alternatives to fossil fuels and to advance energy conversion technologies. Recent decades have seen extensive exploration of renewable energy sources, including wind, solar, and tidal energy. However, the intermittent nature of these sources poses challenges in meeting immediate energy demands.[1–3] Hydrogen energy, an efficient and clean secondary energy source, shows promise as a key component of future energy systems due to its sole combustion byproduct being water.[4–7] Despite its advantages, H_2 presents challenges for storage and transportation due to its small molecular size, propensity to leak, and the difficulty of liquefaction under normal temperatures and pressures, all of which contribute to increased costs.[8–10] Consequently, it is crucial to develop effective H_2 storage and transport methods. Among the various options, NH_3 has emerged as a promising H_2 carrier, offering a potential solution to these challenges.[11,12]

NH_3 is a nitrogenous compound comprising one nitrogen atom and three hydrogen atoms. It can be readily liquefied under ambient conditions, offering significant economic and safety benefits for storage and transportation. With an exceptional volumetric energy density of 12.9 MJ L^{-1}, NH_3 significantly outperforms liquid H_2 (8.6 MJ L^{-1}), making it an attractive option for energy storage.[13,14] Moreover, global NH_3 production exceeds 170 million tons annually, supported by a well-established, cost-effective production and supply chain. The mature technology for NH_3 synthesis, combined with its ideal combustion products being primarily N_2 and water without CO_2 emissions, underscores its potential to mitigate global

Mingzhuang Liang

Mingzhuang Liang obtained his PhD in Chemical Engineering from Nanjing Tech University, China, under the supervision of Prof. Zongping Shao. He is currently a Postdoctoral Fellow at Seoul National University. His research interests are mainly focused on the development of key materials for applications in solid oxide cell.

Jinwook Kim

Jinwook Kim is currently a Postdoctoral Fellow at the School of Materials Science and Engineering, at Northwestern University, USA. He received his PhD in Materials Science and Engineering from Korea Advanced Institute of Science and Technology, Korea, in 2023. His research interest focuses on the fabrication and characterization of novel solid oxide fuel cell electrodes for efficient energy storage and conversion.

Tae Ho Shin

Tae Ho Shin is a Director and Principal researcher for Division of Carbon Neutrality & Materials Digitalization at Korea Institute of Ceramic Engineering and Technology (KICET). He received his PhD at Kyushu University, Japan. He worked as Research Fellow in the School of Chemistry at the University of St Andrews, and he then joined KICET, Korea (2015). His research involves developing new oxide electrodes for electrochemical devices such as solid oxide fuel cells and electrolysis cells. An area of particular interest is crystal structure analysis for understanding and predicting the design of materials with targeted electrochemical properties.

Zongping Shao

Zongping Shao is a John Curtin Distinguished Professor at Curtin University, Australia. He obtained his PhD from Dalian Institute of Chemical Physics, China, in 2000. He worked as a visiting scholar at the Institute Researches Sur La Catalyse, CNRS, France, and then a postdoctoral fellow at California Institute of Technology, USA, from 2000 to 2005. His research interests include mixed conducting membranes, solid oxide electrochemical cells, electrocatalysis, advanced energy storage devices including lithium/sodium-(ion) batteries, metal–air batteries, supercapacitors, and solar cells. He has been recognized as a Highly Cited Researcher by Clarivate Analytics since 2017.

climate change. These characteristics position NH_3 as a promising clean fuel and H_2 carrier. The Haber–Bosch process, the current dominant method for NH_3 synthesis, requires high temperatures (400–500 °C) and pressures (150–350 atm) to drive the reaction between N_2 and H_2 over an iron-based catalyst.[15,16] However, this process has significant drawbacks, including substantial energy consumption (1–2% of global energy consumption from steam-methane reforming), considerable CO_2 emissions (~1.8% of global CO_2 emissions), and the high equipment and maintenance costs associated with such extreme operating conditions. Moreover, the H_2 required for this process is typically derived from methane, further leading to substantial carbon emissions.[17,18] Consequently, alternative NH_3 synthesis methods, including electrochemical approaches, plasma techniques, and solid nitride cycling, have attracted considerable interest.[18–20] Among these, electrochemical approaches, with their potential for seamless integration with renewable energy systems, are the most promising technologies for sustainable NH_3 production. Based on the operating temperature, electrochemical NH_3 synthesis devices can be categorized into low-temperature (<100 °C), intermediate-temperature (200–600 °C), and high-temperature (>700 °C) systems.[21] Compared to other low- and intermediate-temperature devices such as alkaline water electrolyzers and proton exchange membrane electrolyzers, solid oxide electrolysis cells (SOECs) typically require fewer noble metal catalysts, exhibit faster reaction rates, and achieve higher energy efficiency.[22–24]

Solid oxide cells (SOCs), encompassing both SOECs and solid oxide fuel cells (SOFCs), are an emerging technology for energy conversion and storage.[25–27] These cells offer the versatility to switch between electrolysis cell and fuel cell modes, facilitating the efficient interconversion between electrical and chemical energy.[28–30] This reversible-mode capability positions SOCs as a promising technology for enhancing the flexibility, stability, and sustainability of energy systems, marking them a key focus for future energy research. SOCs are categorized based on the type of charge carrier in their electrolytes: oxygen ion conducting SOCs (O-SOCs) and protonic ceramic cells (PCCs).[31,32] PCCs typically operate at intermediate to low temperatures (<600 °C) due to the relatively low activation energy required for proton transport compared to oxygen ion transport.[33] PCCs can function in two modes: protonic ceramic electrolysis cells (PCECs) and protonic ceramic fuel cells (PCFCs). In PCEC mode, excess renewable electricity can be utilized for NH_3 synthesis and storage.[34,35] Conversely, PCFCs can convert stored NH_3 back into electricity to meet immediate energy demands.[36,37] Despite the potential of PCCs, challenges remain in the electricity-to-NH_3 interconversion, particularly related to catalyst stability and efficiency, material and manufacturing costs, and the optimization of reaction conditions.[38–41] Overcoming these challenges is crucial for advancing the practical application of PCCs in future energy systems.

Numerous studies have previously been published, focusing on the development of electrolytes, electrode catalysts, and operating conditions for NH_3 synthesis in PCCs and direct NH_3-fueled proton ceramic fuel cells (DA-PCFCs). This review begins by outlining the fundamental mechanisms involved in electricity-to-NH_3 interconversion in PCCs, followed by a detailed analysis of the challenges associated with achieving such conversions. Subsequently, the advancements and achievements in electricity-to-NH_3 interconversion using PCCs over the past few decades are summarized. Finally, the review concludes with a forward-looking perspective on the future applications of PCCs in electricity-to-NH_3 interconversion, highlighting the critical role they could play in shaping next-generation sustainable energy systems. By providing an in-depth examination of the state of the art, the objective of this review is to serve as a comprehensive guide for researchers engaged in the advancement of proton-conducting ceramic technologies, addressing both the current obstacles and potential breakthroughs that could drive innovation in clean energy conversion, which is critical for accelerating the transition to a sustainable and carbon-neutral global energy landscape.

WooChul Jung

WooChul Jung is an Associate Professor at Seoul National University, Korea. He received his PhD degree at MIT and served as a postdoctoral fellow at Caltech. The main goal of his research activities is to understand the reactions that occur at the interfaces between ionic solids (oxides in particular) and gases and thereby to improve the reaction kinetics for applications in chemical and electrochemical catalysis, such as, solid oxide fuel cells, electrolyzers, and hydrocarbon reformers. He has been developing model oxide structures with well-defined interface geometries and analyzing true surface properties and reaction characteristics.

2. Mechanisms of the electricity-to-NH_3 interconversion in PCCs

2.1. NH_3 synthesis in PCECs

PCECs have been employed for NH_3 synthesis through various electrochemical processes, with the goal of achieving reactors that offer high energy efficiency and minimal greenhouse gas emissions.[38,42,43] Currently, three main types of PCEC reactors are utilized for NH_3 synthesis, each based on different reactions: the hydrogen oxidation reaction (HOR), methane-steam reforming reaction (MSRR), and water oxidation reaction (WOR), as illustrated in Fig. 1. In the following sections, we will examine the operating mechanisms of these reactors and discuss the challenges in NH_3 synthesis by PCECs.

In Reactor 1, H_2 is supplied to the anode, while N_2 is introduced at the cathode (Fig. 1a). Under an applied voltage, H_2 molecules dissociate into protons and electrons ($H_2 \rightarrow 2H^+ + 2e^-$). The generated protons then migrate across the electrolyte to the cathode and combine with adsorbed nitrogen to produce NH_3 ($6H^+ + N_2 + 6e^- \rightarrow 2NH_3$).[44,45] This approach offers significant advantages over the traditional high-pressure NH_3 synthesis methods, as it operates under moderate conditions and directly converts electrical energy into chemical energy. However, a primary challenge lies in the need for a reliable H_2 source. Consequently, Reactor 1 must be coupled with H_2 production systems, such as methane reforming or water electrolysis, which significantly increases the overall system cost.

Reactor 2, a more integrated approach, utilizes renewable electricity to reform methane and water steam into H_2 and CO_2 on the anode side (Fig. 1b).[46,47] The protons from H_2 dissociation then migrate across the electrolyte to the cathode, combining with adsorbed nitrogen to form NH_3. Unlike Reactor 1, Reactor 2 eliminates the need for additional H_2 production equipment, greatly simplifying the overall system. By combining the endothermic reforming reaction with the exothermic nitrogen reduction, Reactor 2 achieves a thermoneutral state, enhancing energy efficiency. Additionally, the generated CO_2 can be further reformed with methane to produce CO, reducing carbon emissions. However, the anode's exposure to methane, steam, and CO_2 necessitates a stable and highly active electrode material to ensure optimal performance and longevity. Fortunately, numerous methane steam reforming anode catalysts developed for SOFCs can be adapted for use in Reactor 2.[48–50]

Recent advancements in PCECs have enabled efficient H_2 production through water electrolysis. Therefore, researchers have increasingly explored PCECs for a more environmentally friendly approach to NH_3 synthesis (Fig. 1c).[51,52] In Reactor 3, the WOR at the anode is driven by renewable electricity, leading to the generation of protons and oxygen. These protons migrate through the electrolyte to the cathode, where they react with absorbed nitrogen to form NH_3.[52,53] This process, utilizing only water and N_2, offers a carbon-free pathway for NH_3 production. To ensure optimal performance and longevity in the high-steam environment required for Reactor 3, the development of advanced anode materials is crucial. Fortunately, some anode materials already used in PCEC water electrolysis for H_2 production, such as $PrBa_{0.5}Ca_{0.5}Co_2O_{5+\delta}$ (PBCC), $Ce_{0.2}Ba_{0.2}Sr_{0.2}La_{0.2}Ca_{0.2}CoO_{3-\delta}$ (CBSLCC), and $BaCo_{0.4}Fe_{0.4}Zr_{0.1}Y_{0.1}O_{3-\delta}$ (BCFZY), are also well-suited for this NH_3 production process.[54–56]

In all the three pioneering NH_3 synthesis reactors, despite varying anode reactions, the cathode, where the nitrogen reduction reaction (NRR) takes place, shares a striking resemblance. Currently, there are three main NRR mechanisms, as illustrated in Fig. 1d–f. In Fig. 1d, the NRR within the PCEC reactor proceeds *via* a dissociative mechanism. Initially, N_2 molecules are adsorbed onto the catalyst surface, undergoing subsequent activation. Subsequently, hydrogen protons from the anode and electrons combine with the activated nitrogen in a hydrogenation process to form NH_3. Finally, the NH_3 molecules desorb from the catalyst surface.[57,58] Owing to the substantial energy barrier for N_2 dissociation on the catalyst surface, this step is generally regarded as the rate-determining step (RDS) in NH_3 synthesis. Consequently, promoting N_2 dissociation can effectively enhance NH_3 production rate.[59,60] Fig. 1e and f depict the NRR associative mechanism, further categorized into alternating and distal hydrogenation pathways based on distinct hydrogenation sequences.[61] In Fig. 1e, a N_2 molecule initially adsorbs onto the catalyst surface. Hydrogenation occurs preferentially at the distal nitrogen atom of the adsorbed N_2 molecule. This stepwise hydrogenation process culminates in the formation of an NH_3 molecule, which then desorbs from the catalyst surface. Subsequent

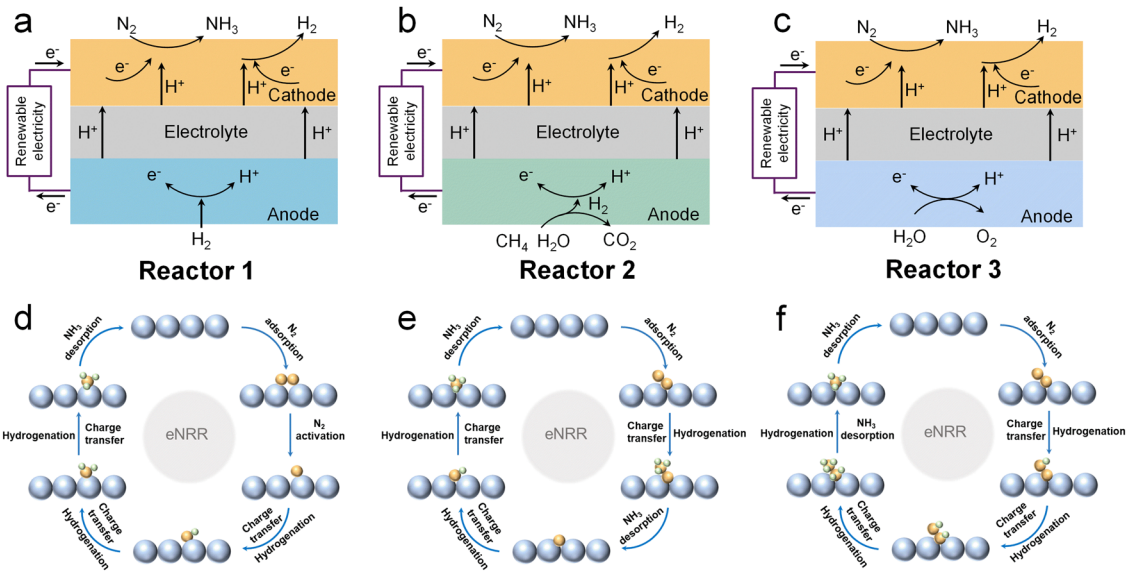

Fig. 1 The PCC reactors for NH_3 synthesis *via* (a) HOR, (b) MSRR and (c) WOR. (d)–(f) The potential mechanisms of the NRR.

hydrogenation of the remaining nitrogen atom completes the catalytic cycle, yielding a second NH_3 molecule that desorbs from the catalyst surface.[21] Conversely, in Fig. 1f, both N atoms of the adsorbed N_2 molecule experience sequential hydrogenation. When the distal nitrogen atom reaches the NH_3 state and desorbs, the proximal nitrogen atom continues to be hydrogenated until it also forms NH_3 and desorbs.[62] Consequently, for the associative mechanism, enhancing adsorbed N_2 activation significantly augments NH_3 synthesis rates *via* NRR.[63,64] Unlike ambient temperature processes, the elevated operating temperature of PCECs (300–600 °C) promotes the dissociation of the strong N≡N bond, a critical step in NH_3 synthesis. To elevate the electricity-to-NH_3 conversion rate, developing cathodes with exceptional NRR activity is paramount. The PCEC reactor's cathode typically consists of metal nanoparticles supported on an oxide, which is conducive to the NRR process.[38,65,66] The catalytic activity of catalysts for the NRR in PCECs is generally influenced by their electronic structure, crystal structure, and surface morphology.[67,68] Moreover, different preparation methods can significantly affect the catalyst's particle size, dispersion, and specific surface area, thus impacting its catalytic performance.

2.2. Direct NH_3 utilization in PCFCs

PCFCs exhibit excellent fuel flexibility, enabling the utilization of electrochemically produced NH_3 for power generation. In DA-PCFCs, water steam is generated at the cathode, preventing dilution of the fuel gas at the anode, thus enhancing fuel utilization.[69–71] Additionally, the electrolyte effectively separates oxygen ions from NH_3, preventing the formation of NO_x.[72,73]

In DA-PCFCs, the NH_3 molecule is initially adsorbed onto the anode surface and dissociates into H_2 and N_2. Subsequently, the electrochemical process involves the oxidation of H_2 at the anode, generating protons. These protons are conducted through the electrolyte to the cathode, where they participate in the reduction of oxygen to form H_2O (Fig. 2a).[74] An effective anode catalyst enhances NH_3 decomposition by providing a greater number of active sites for adsorption and subsequent decomposition.[75,76] An ideal anode catalyst should possess high NH_3 adsorption capacity, low N–H bond dissociation energy, and excellent resistance to poisoning.[77,78] To date, a diverse array of anode catalysts has been developed, encompassing noble metal-based catalysts (Pt, Pd, Ru, *etc.*), transition metal oxide catalysts (Ni, Co, Fe, *etc.*), and metal-ceramic catalysts (Ni–BZCY, Ni–BZCYYb, $Sr_2CoMo_{0.8}Ni_{0.2}O_{6-\delta}$ *etc.*).[79–82] The catalytic activity of these catalysts is influenced by a complex interplay of factors, including their electronic structure, surface properties, and the nature of their interactions with the support material.

NH_3 decomposition at the anode surface is a complex process involving the following steps:[83,84]

$$NH_3\ (g) + * \leftrightarrow NH_3*$$

$$NH_3* + * \rightarrow NH_2* + H*$$

$$NH_2* + * \rightarrow NH* + H*$$

$$NH* + * \rightarrow N* + H*$$

$$2H* \rightarrow H_2\ (g) + 2*$$

$$2N* \rightarrow N_2\ (g) + 2*$$

wherein, the reaction site for NH_3 decomposition is denoted by "*". The nitrogen atoms in NH_3 molecules are initially adsorbed at the active sites of the PCFC anode. Subsequently, the N–H bonds undergo cleavage, leading to the release of H_2 molecules. Finally, following recombination of adjacent nitrogen atoms into nitrogen molecules, the newly formed molecules desorb from the surface (Fig. 2b). The kinetics of NH_3 decomposition on metal sites (M) is strongly influenced by the strength of the bond formed between the metal and nitrogen atoms (M–N). While a stronger M–N bond promotes the breaking of N–H bonds, it also hinders the release of N_2 molecules from the catalyst surface. Conversely, a weaker M–N bond facilitates the release of N_2, it impedes the breaking of N–H bonds.[85,86] Consequently, optimizing the M–N bond strength is essential for enhancing NH_3 decomposition. The RDS for NH_3 decomposition is generally considered to be N–H bond cleavage on noble metals such as Ru and Pd due to their strong H_2 adsorption capabilities, which facilitate the formation of stable metal–H bonds and inhibit further N–H bond cleavage.[87] For non-noble metals like Fe, Co, and Ni, the N_2 desorption is considered to be the RDS. This is attributed to the relatively strong interaction between N_2 and these metals, making it difficult for N_2 molecules to desorb from the catalyst surface. However, the electronic structure of the catalyst and the

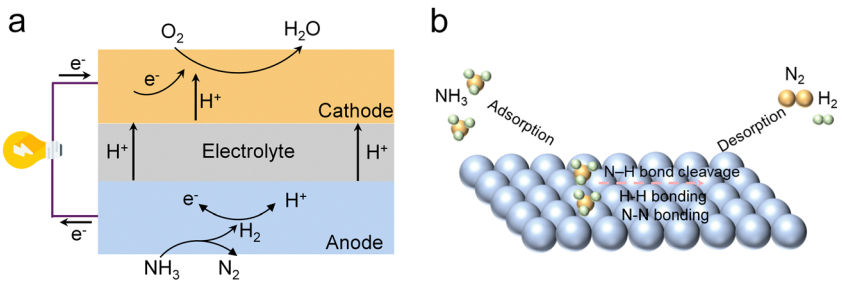

Fig. 2 (a) Schematic illustration of the operating mechanism of the DA-PCFC. (b) The mechanism of NH_3 decomposition on the anode side.

properties of the support can influence the nature of the active sites and thus alter the RDS.[83,85] Therefore, the RDS of NH_3 decomposition is dependent on the nature of the catalyst.

3. Challenges of electricity-to-NH_3 interconversion in PCCs

3.1. NH_3 synthesis in PCECs

Research and development of PCEC technology for NH_3 synthesis is currently in its nascent stages, with significant potential for future advancements. However, achieving high faradaic efficiency (FE) for NH_3 synthesis remains a critical challenge for the advancement of PCEC technology, primarily due to the competitive relationship between the hydrogen evolution reaction (HER) and the NRR.[88] This competition is influenced by various factors, including the applied potential, local reactant availability (H^+/N_2), and the characteristics of the PCEC cathode, which determine the binding of reactants and electron transfer.[89] Although higher temperatures can promote N_2 dissociation and adsorption, they can also induce NH_3 decomposition, leading to a decrease in FE. Thus, precise control of the reaction temperature is essential.[67,68] In the reactor depicted in Fig. 1a, the NH_3 yield can be significantly enhanced by adjusting the partial pressures of H_2 and N_2.[90,91] Additionally, numerous strategies have been reported to modify the electronic structure and increase the active sites of NRR catalysts, including tailoring the size and morphology, elemental doping, and introducing defects, which can enhance the FE of NH_3 production in PCECs.[22,92,93] Although reported NH_3 synthesis rates (10^{-13} to 10^{-8} mol cm^{-2} s^{-1}) surpass those of low-temperature electrochemical methods (<100 °C), the low FE remains a hurdle for practical implementation. Therefore, rational design of both the cathode and reaction conditions is imperative for advancing PCEC NH_3 synthesis technology.

3.2. Direct NH_3 utilization in PCFCs

Despite the significant advantages of DA-PCFCs, their practical implementation is currently hindered by insufficient stability and suboptimal low-temperature performance.

3.2.1. Limited power densities at low temperatures. At present, DA-PCFCs exhibit limited power densities at low temperatures (<500 °C), primarily stemming from the increased ohmic resistance of the electrolyte, sluggish oxygen reduction kinetics at the cathode, and poor anode performance in NH_3 decomposition at low temperatures. Novel thin-film electrolyte fabrication techniques, such as pulsed laser deposition, tape-casting and spin coating, enable the preparation of thin electrolyte layers (<10 μm), significantly reducing the ohmic resistance.[94–96] The sluggish oxygen reduction kinetics leads to a drastic increase in the polarization resistance of the cathode at decreased temperatures, thus degrading the performance of DA-PCFCs. Advanced triple-conducting cathodes, such as $BaCo_{0.4}Fe_{0.4}Zr_{0.1}Y_{0.1}O_{3-\delta}$, $BaCo_{0.8}Ta_{0.2}O_{3-\delta}$, and $PrBa_{0.8}Ca_{0.2}Co_2O_{5+\delta}$, have demonstrated excellent electrochemical activity in H_2-fueled PCFCs and show promise as potential cathode materials for DA-PCFCs.[54,97,98] The poor NH_3 decomposition performance of most of the DA-PCFC anodes or anode catalytic layers at low temperatures severely compromises the open-circuit voltage and power density of DA-PCFCs.[99,100]

3.2.2. Poor durability. When DA-PCFCs operate at low temperatures, the Ni-based anode, due to its insufficient activity, cannot completely decompose NH_3 into N_2 and H_2, leading to the nitridation of Ni particles to form nickel nitride ($NH_3 + 3Ni \rightarrow Ni_3N + 1.5H_2$).[101,102] However, Ni_3N is unstable under H_2 conditions and can be reduced back to Ni.[11] This process leads to microstructural changes within the DA-PCFC anode, specifically at the interface with the electrolyte. These changes increase the interfacial polarization resistance, hindering efficient charge transfer at the interface, thereby causing cell degradation and even electrolyte cracking. To address this issue, researchers have proposed adding additional NH_3 crackers or an anode catalyst layer. This can decompose most of the NH_3 before it reaches the Ni-based ceramic anode of the DA-PCFCs, effectively reducing the contact between the Ni-based ceramic anode and high-concentration NH_3, thereby improving the operational stability of the DA-PCFCs.[103–106] Furthermore, NH_3 decomposition is an endothermic process. Non-uniform temperature distribution during NH_3 decomposition can induce thermal stresses within the cell, resulting in severe performance degradation, which is particularly pronounced in cell stacks.[101] Additionally, the mismatch in thermal expansion coefficients (TECs) among different components makes DA-PCFCs susceptible to performance degradation during rapid thermal cycling.[107] In 2021, Shao *et al.* introduced a negative thermal expansion compensation strategy and incorporated the negative thermal expansion oxide $Y_2W_3O_{12}$ (TEC = -7×10^{-6} K^{-1}) into the oxide $SrNb_{0.1}Co_{0.9}O_{3-\delta}$ (TEC = 20.5 × 10^{-6} K^{-1}) to successfully develop a SOFC cathode $SrWO_4$–$Sr_x(Y_y(Nb_{0.1}Co_{0.9})_{1-y})O_{3-\delta}$ with a low TEC (12.9 × 10^{-6} K^{-1}), effectively improving the thermal cycling stability of SOFCs.[108] Recently, Chen *et al.* impregnated $Ru_{0.95}Cu_{0.05}$ into the anode skeleton of DA-PCFCs to prepare $Ru_{0.95}Cu_{0.05}Ni_x$–Ni–$BaZr_{0.1}Ce_{0.7}Y_{0.1}Yb_{0.1}O_{3-\delta}$ (RCN–Ni–BZCYYb) anode catalysts, significantly improving the thermal cycling stability of DA-PCFCs.[99] Therefore, for DA-PCFCs supported by Ni-based ceramic anodes, developing catalysts with high catalytic activity for NH_3 decomposition, either as an anode catalytic layer or for additional NH_3 crackers, is of profound significance for improving the stability of DA-PCFCs. Additionally, developing electrodes that are compatible with the electrolytes' TEC is equally important for improving the thermal cycling stability of DA-PCFCs.

4. Recent advances

4.1. NH_3 synthesis in PCECs

Recent advances in PCEC NH_3 synthesis research can be grouped into three main approaches: hydrogen-based, methane-based, and water-based synthesis. Each approach presents unique advantages and challenges, and the focus of

research varies based on the materials used. Hydrogen-based synthesis has garnered the most attention due to its simple system and relatively established pathways.[109] Researchers are mainly focusing on optimizing the NRR catalyst to enhance overall efficiency and NH_3 selectivity. Methane-based synthesis is less explored but presents a unique advantage in reducing the complexity of the reactor system.[110] Since methane can be directly reformed to produce H_2, it eliminates the need for separate reformers or other processing units, which can reduce both the size of the overall system and streamline the synthesis process by decreasing the number of required steps. This streamlined process has the potential to lower costs and simplify industrial-scale implementation, making it a promising alternative for future research. However, not only the NRR but also the methane-steam reforming reaction (MSRR) should be considered, and the selection of materials are limited due to carbon coking.[48,111,112] Water-based synthesis represents the ultimate goal for a fully sustainable NH_3 production method.[113] This approach offers a sustainable pathway for NH_3 synthesis by utilizing water as the source of protons and nitrogen from the air, eliminating carbon emissions and relying solely on abundant resources. However, water-based synthesis currently faces significant challenges, particularly in terms of energy consumption and reaction efficiency. Despite these obstacles, the potential environmental benefits have spurred considerable research activity, and advancements in catalyst and cell design are steadily addressing the technical hurdles.

4.1.1. NH_3 synthesis *via* the hydrogen oxidation reaction (HOR). NH_3 synthesis using the HOR in PCECs has been explored since the early stages of PCEC research. Initially, metal electrodes such as Pd were used to facilitate NH_3 synthesis due to their proven electrochemical activity.[114] Early study with Pd electrodes by Marnellos *et al.* in 1998, demonstrated the feasibility of PCEC for NH_3 production, laying the groundwork for further development.

As PCEC research progressed, the development of highly active triple-conducting oxides (TCO) significantly advanced the field.[5,98] These materials, which can conduct protons, oxygen ions, and electrons or holes, have been widely adopted to increase cell performance from wide active reaction sites. Therefore, several studies were conducted by using TCO material as the PCEC electrode for NH_3 production.[115] However, in the case of NH_3 production, simply achieving high current densities is not sufficient; NH_3 selectivity is equally critical. To improve selectivity for NH_3 synthesis, many studies have introduced catalysts like Ru, which is known for its high NRR activity and selectivity.[65,116–119] Ru-based catalysts, especially when used in exsolution techniques, allow for efficient catalyst utilization even in small quantities. However, the high cost of precious metals such as Ru presents a challenge, even when used in small amounts, as it significantly raises the overall cost of the electrode. In an effort to overcome this limitation, researchers have explored the use of alternative materials, including transition metals like Fe, Co, and Ni.[38,39,44,66,68,115,120,121] These metals have shown promise as catalysts for NH_3 synthesis, offering a cost-effective solution while maintaining reasonable activity.

More recently, perovskite electrodes have garnered attention for their potential in NH_3 synthesis.[22,67,68] The $La_{0.9}Bi_{0.1}FeO_{3-\delta}$ (LBiF) perovskite was prepared by Chen *et al.* and was used as a cathode in a PCEC to realize NH_3 synthesis (Fig. 3a and b).[67] The introduction of Bi dopants resulted in the formation of new $Bi^{3+}/Bi^{2+}/Bi^0$ redox electron pairs, which facilitated electron transfer and thereby improved the electrical conductivity of the material (Fig. 3c). Furthermore, Bi significantly boosted the NRR activity and effectively suppressed the HER. When LBiF was used as the NRR electrocatalyst, the faradaic efficiency (FE) for NH_3 synthesis reached a maximum value of 2.03% at 650 °C and 0.4 V, with an NH_3 production rate of 4.47×10^{-9} mol cm^{-2} s^{-1}, surpassing that of $LaFeO_{3-\delta}$ (LF), $La_{0.9}FeO_{3-\delta}$ ($L_{0.9}F$), and LBi (Fig. 3d and e). In their other research, an NRR electrocatalyst, $LaCu_{0.1}Fe_{0.9}O_{3-\delta}$ (LCuF), for NH_3 synthesis in a PCEC was fabricated by Cu doping (Fig. 3f).[68] The synergistic effect of Cu and Fe facilitates electron transfer through the Fe–$O^{2-\delta}$–Cu pathway, enriching Fe sites with Fe^{4+} and Cu sites with Cu^+. This enhanced electron transfer kinetics boosts NRR performance. At an operating temperature of 650 °C and a cell voltage of 0.4 V, the PCEC with the LCuF electrode achieved a FE of 2.8% and an NH_3 production rate of 5.12×10^{-9} mol cm^{-2} s^{-1} (Fig. 3g and h). Furthermore, they prepared $Sr_{0.9}Ti_{0.6}Fe_{0.4}O_{3-\delta}$ ($S_{0.9}TF$) *via* A-site defect engineering. The abundant oxygen vacancies, Ti^{3+} species, and exsolved Fe active particles enhanced N_2 adsorption and activation, improving NRR activity. At 650 °C and 0.6 V, PCEC with $S_{0.9}TF$ exhibited a maximum NH_3 production rate of 6.84×10^{-9} mol cm^{-2} s^{-1} and a FE of 2.79%. Through a simple B-doping method, they synthesized a synergistic mixed catalyst, $Sr(Ti_{0.6}Fe_{0.4})_{0.8}B_{0.2}O_{3-\delta}$, composed of $Sr_3B_2O_6$ (SB) and $Sr_{1-y}Ti_{0.6}Fe_{0.4}O_{3-\delta}$ ($S_{1-y}TF$).[122] SB acts as a proton acceptor, effectively suppressing the HER and promoting proton-coupled electron transfer for NH_3 synthesis. Furthermore, the grain boundaries between $S_{1-y}TF$ and SB introduce more defects, significantly enhancing the NH_3 production rate and FE. In these reports, the NH_3 content was quantified using the indophenol blue method, which detects NH_3 by forming a blue-colored complex with phenol and hypochlorite under alkaline conditions, measured spectrophotometrically to determine the NH_3 concentration.

While most research has focused on NRR electrodes and catalysts, recent studies have also investigated the role of electrolytes in enhancing NH_3 synthesis. An ideal PCEC electrolyte should exhibit high proton conductivity. In the NH_3 synthesis process, H_2 is supplied electrochemically in the form of protons.[123] Therefore, the H_2 supply rate is limited by the maximum proton flux. In the early stages of PCEC NH_3 production research, Ma *et al.* synthesized cubic perovskite $BaCe_{0.85}Y_{0.15}O_{3-\delta}$ (BCY15) samples *via* a microemulsion method, exhibiting nearly pure proton conductivity in wet H_2. Cavity ring-down spectroscopy was employed to quantify NH_3 production in a symmetric Ag–Pd electrode cell with a BCY15 electrolyte. By measuring the ring-down time of a laser beam in an optical cavity, shortened by NH_3 absorption, this technique enables the detection of exceedingly low NH_3 concentrations. Under an applied current of 0.75 mA and a temperature of

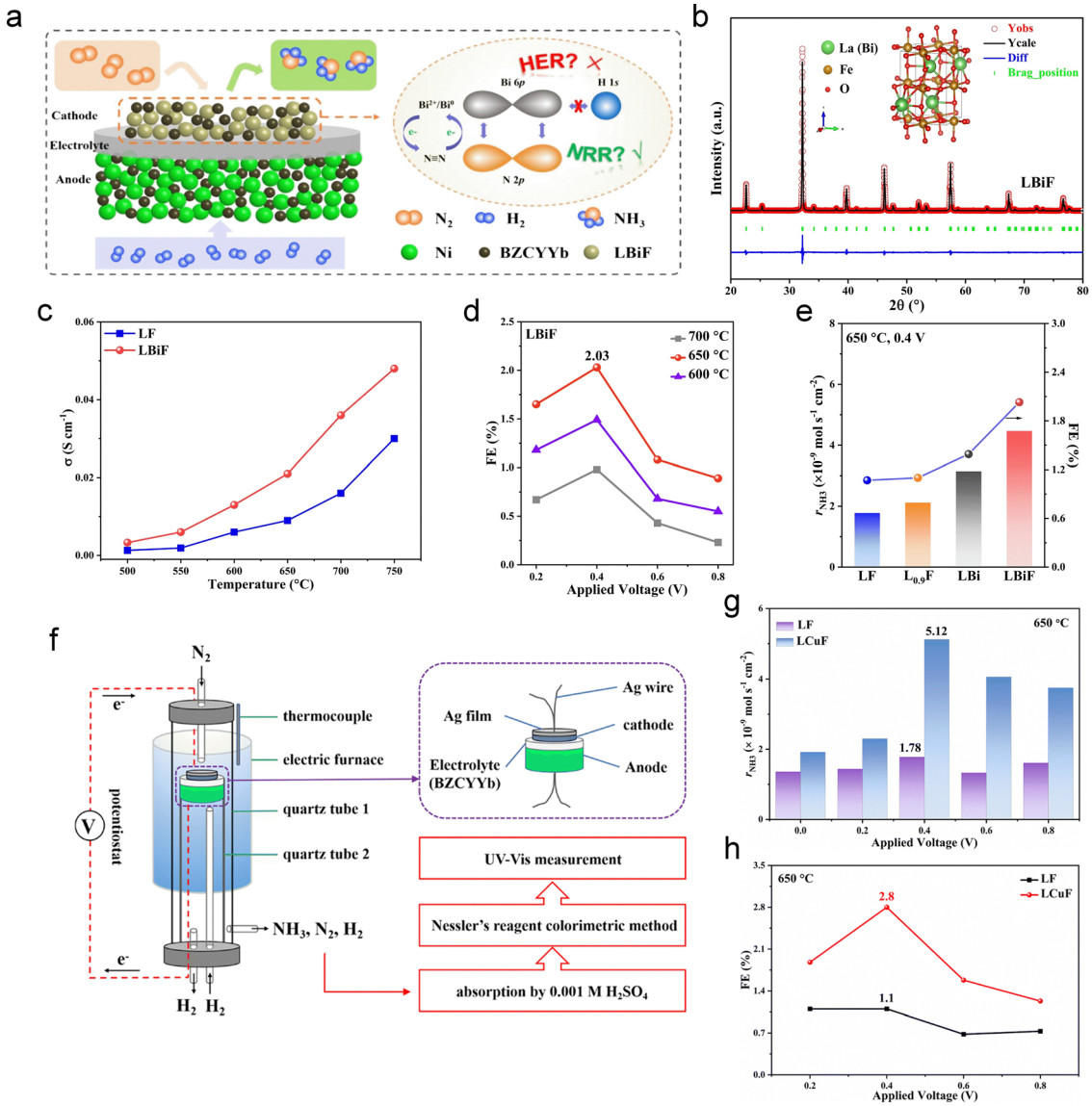

Fig. 3 (a) Schematic of NH_3 synthesis in PCEC with the LBiF electrode. (b) Rietveld refined XRD pattern of LBiF. (c) Electrical conductivities of LF and LBiF in 10% H_2 + 90% N_2. (d) The FE values and (e) NH_3 production rate in PCEC with the LBiF electrode. Reproduced with permission.[67] Copyright 2024, Elsevier. (f) Schematic diagram of the NH_3 synthesis device. (g) The FE values and (h) NH_3 production rate in PCEC with the LCuF electrode. Reproduced with permission.[68] Copyright 2024, Royal Society of Chemistry.

500 °C, a maximum NH_3 synthesis rate of 2.1×10^{-9} mol s^{-1} cm^{-2} was achieved.[124] Other Ba-based electrolytes, such as $BaZr_{0.8}Y_{0.2}O_{3-\delta}$, $BaCe_{0.65}Zr_{0.2}Er_{0.15}O_{3-\delta}$, $BaCe_{0.2}Zr_{0.7}Y_{0.1}O_{3-\delta}$, and $BaZr_{0.1}Ce_{0.7}Y_{0.1}Yb_{0.1}O_{3-\delta}$, have been extensively studied.[109,123,125,126] More recently, Wang *et al.* developed cells using $La_{5.5}WO_{11.25-\delta}$ (LWO) electrolyte instead of the traditional Ba-rich materials (Fig. 4a).[45] LWO electrolyte possesses high stability under CO_2 conditions and unique conductivity properties.[127,128] This high proton conduction ensures that activated protons can efficiently participate in the NRR, leading to enhanced NH_3 production without compromising the FE. Consequently, the LWO electrochemical membrane reactor demonstrated superior performance across a wide temperature range. Quantitative analysis of NH_3 production was conducted using the indophenol blue method. Its FE and NH_3 production rate surpassed those of most other electrochemical NH_3 synthesis systems, including those operating at room temperature with Ru-based catalysts and those at elevated temperatures above 500 °C (Fig. 4b). Furthermore, the reactor demonstrated excellent stability, maintaining a consistent NH_3 production rate and FE over long-term testing at 350 °C (Fig. 4c). This durability, along with its enhanced performance, makes LWO a highly promising material for use in PCEC NH_3 synthesis.

4.1.2. NH_3 synthesis *via* the methane-steam reforming reaction (MSRR). While the ideal method for NH_3 synthesis involves using H_2 or water to minimize CO_2 emissions, the reality is that the dominant origin of H_2 production is still achieved through steam methane reforming. This H_2 is then

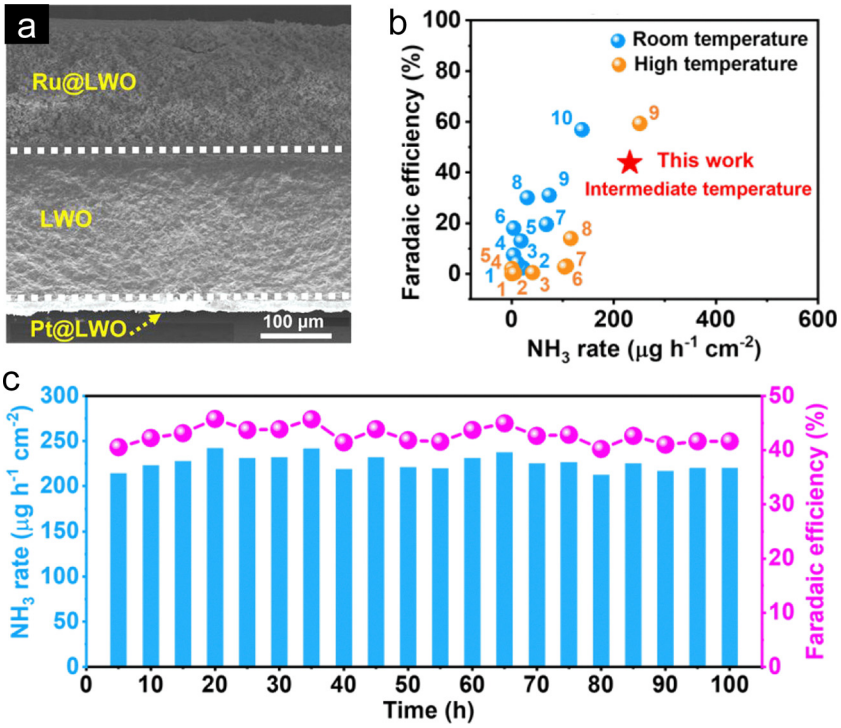

Fig. 4 (a) Cross-section SEM image of the LWO membrane reactor. (b) Comparison NH_3 production rate and FE of the LWO membrane reactor with other reference data. (c) Long-term stability of the LWO membrane reactor at 2500 μA cm^{-2} and 350 °C. Reproduced with permission.[45] Copyright 2023, Cell Press.

typically used in the Haber–Bosch process for NH_3 production. Given this, synthesizing NH_3 directly from methane reforming presents a practical eco-friendly approach in the short to medium term until green H_2 production becomes more cost-competitive and widespread. Methane reforming-based NH_3 synthesis could therefore serve as a practical bridge toward green NH_3 production.

The study by Stoukides *et al.* presents an approach that combines methane reforming reaction and NH_3 synthesis in a protonic ceramic membrane reactor.[129] Fig. 5a shows the integrated cell used for NH_3 synthesis *via* methane reforming reaction. The system combines the vanadium nitride–iron (VN–Fe) cathode and Ni–$BaZr_{0.7}Ce_{0.2}Y_{0.1}O_{3-\delta}$ (Ni–BZCY72) anode with a $BaZr_{0.8}Ce_{0.1}Y_{0.1}O_{3-\delta}$ (BZCY81) electrolyte, facilitating both NH_3 synthesis and methane reforming reactions. This integration simplifies the process by combining methane reforming and NH_3 synthesis in a single reactor unit. Fig. 5b–g present the results of the study, displaying CH_4 conversion, CO_2 selectivity, H_2 production rate, NH_3 production rate, FE for NH_3 production, and current–voltage characteristics at various operating temperature (550 °C, 600 °C, 650 °C). A maximum NH_3 synthesis rate of 68 mmol NH_3 m^{-2} h^{-1} with a FE of 5.5% was achieved at 600 °C, as determined by the indophenol blue method.

Ding *et al.* developed Ru/$La_{0.25}Ce_{0.75}O_{2-x}$ catalysts *via* hydrothermal treatment, introducing hydroxyl groups and inducing electronic restructuring for PCEC NH_3 synthesis. *In situ* generated Ce^{3+}–OH/Ru sites facilitated N≡N bond cleavage and N–H bond formation, significantly enhancing the NRR process.[110] Fig. 6a illustrates the catalyst synthesis method using a hydrothermal process, which integrates Ru into the $La_{0.25}Ce_{0.75}O_{2-\delta}$ (LDCRu) support to create a catalyst with optimized particle size and surface hydroxyl groups. These modifications enable better NRR activity by creating multiple active sites for NH_3 production. Fig. 6b and c provide cross-sectional images of the constructed PCEC using different materials for each purpose. Fig. 6b shows the Ni–BZCYYb based anode support cell used to facilitate the electrochemical reactions with H_2 fuel, while Fig. 6c displays an electrolyte support configuration. Both setups integrate LDCRu catalysts in the cathode to drive the NH_3 synthesis reactions. Fig. 6d shows the current density as a function of applied bias voltage for different cathodes: $PrBa_{0.5}Sr_{0.5}Co_{1.5}Fe_{0.5}O_{3-\delta}$/Ru (P/Ru), P/LDCRu-D (dry), and P/LDCRu-W (wet). It is evident that the wet-prepared P/LDCRu-W catalyst outperforms the others in terms of current density, indicating the importance of surface hydroxyl groups in facilitating proton transport and NH_3 production. Fig. 6e presents the NH_3 production rate, which was determined using the Nessler reagent colorimetric method. The P/LDCRu-W loaded cell significantly enhances the production rate compared to the P/LDCRu-D loaded cell and the conventional Ru catalyst loaded cell. This finding indicates that the surface hydroxyl groups, which are likely formed during the wet preparation process, play a critical role in facilitating the NRR and enhancing its efficiency. Fig. 6f demonstrates the operational stability of the Ni–BZCYYb/P/LDCRu-W system, where the current density

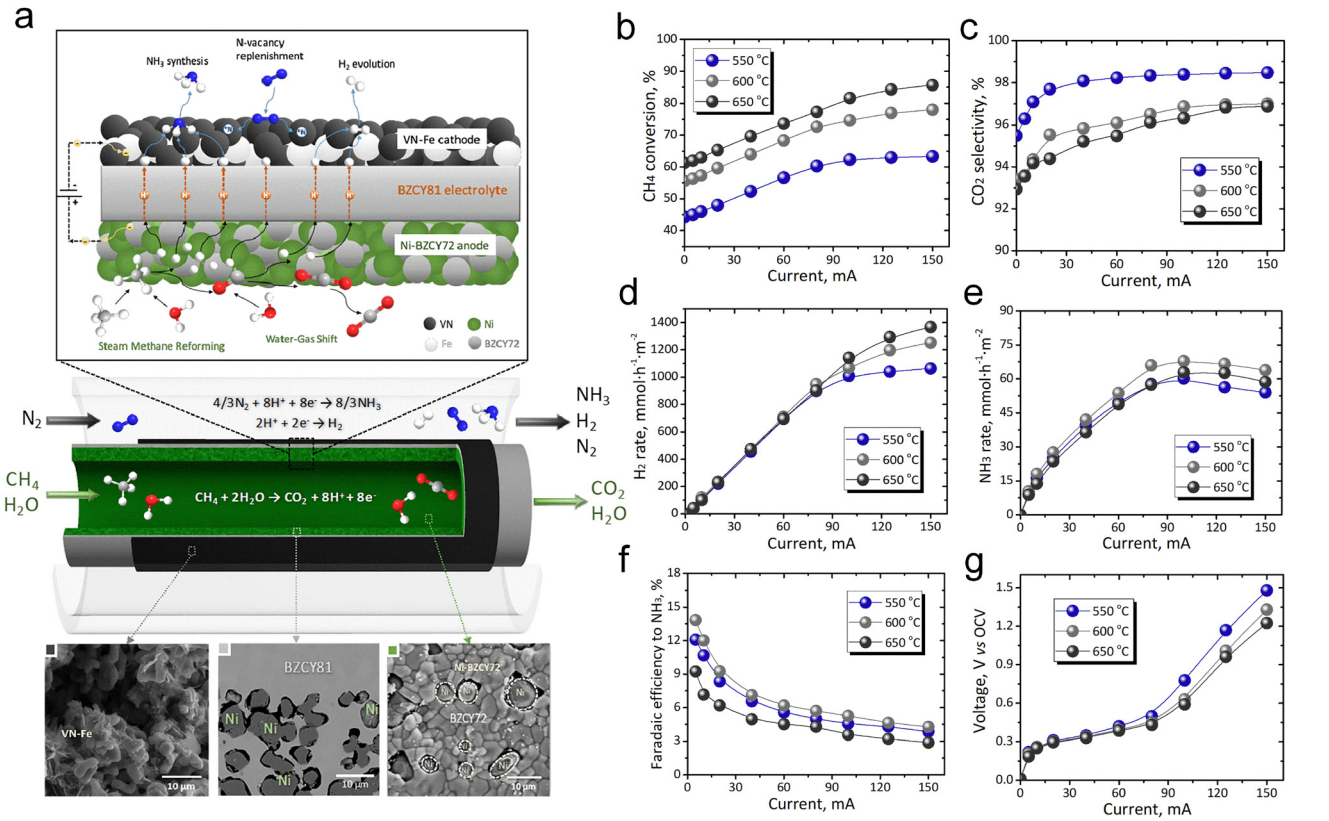

Fig. 5 (a) Schematic and SEM images of the VN–Fe (cathode)/BZCY81 (electrolyte)/Ni–BZCY72 (anode) cell for NH_3 synthesis using methane and steam. Experimental results on (b) CH_4 conversion, (c) CO_2 selectivity, (d) H_2 generated rate, (e) NH_3 synthesis rate, (f) FE to NH_3, and (g) cell voltage *versus* open-circuit voltage as a function of current. Reproduced with permission.[129] Copyright 2020, Cell Press.

remained stable over 550 h at 400 °C. The P/LDCRu-W cathode demonstrated excellent performance, achieving the highest NH_3 production rate of 0.452 mol m^{-2} h^{-1} at an applied voltage of 1.5 V and the highest FE of 36.5% at a lower voltage of 0.6 V (Fig. 6g). They also conducted a similar experiment using C_2H_6 (ethane) as the hydrogen source at the anode. In this case, the highest NH_3 production rate was 0.840 mol h^{-1} m^{-2} at 1.2 V, while the highest FE of 35.0% was achieved at 0.6 V (Fig. 6h). Moreover, the cell with the P/LDCRu-W cathode showed stable FE for NH_3 production under different hydrocarbon gas feeds and operating voltages (Fig. 6i). The results show that the system maintains stable NH_3 production across different conditions, confirming the effectiveness of the Ru/LDC catalyst.

Overall, methane reforming coupled with optimized catalysts constitutes a significant advancement towards efficient and scalable NH_3 synthesis *via* PCEC. While challenges remain, such as improving long-term stability and addressing carbon coking, the advancements highlighted in these studies pave the way for future breakthroughs in NH_3 production.

4.1.3. NH_3 synthesis *via* the water oxidation reaction (WOR). Steam-based NH_3 synthesis using PCECs focuses on using steam at the anode for the WOR and nitrogen at the cathode for the NRR. This method has the advantage of being carbon-free and relies on abundant feedstocks. However, research in this specific configuration remains limited compared to others, such as hydrogen-based approaches. One of the main challenges of steam-based NH_3 synthesis lies in the thermodynamic inefficiency at lower operating temperatures.[35] While converting H_2 and N_2 to NH_3 is more efficient at typical operating temperatures (300–500 °C), the use of steam as a feedstock introduces an energy consumption step due to the endothermic nature of the steam electrolysis reaction. Although less energy-intensive than the traditional Haber–Bosch process, steam-based NH_3 synthesis in PCECs requires more energy compared to alternative PCEC configurations, especially as more energy is required for water electrolysis. Additionally, optimizing not just one electrode, but both the WOR and NRR electrodes as well as the electrolyte simultaneously is crucial for improving the efficiency of steam-based NH_3 synthesis. If either of the electrodes is not optimized, the overall reaction kinetics will be sluggish, leading to reduced performance. Beyond electrode optimization, addressing the durability of the electrolyte and minimizing electronic leakage are also critical. In steam-based PCECs, NH_3 production rates can be lower due to electronic leakage in the electrolyte.[130] This leakage diminishes FE and limits NH_3 production. Therefore, optimizing all system components, including both electrodes and the electrolyte, is essential to fully realize the potential of steam-based NH_3 synthesis. Despite these challenges, efforts to optimize this technology have shown promise, and several

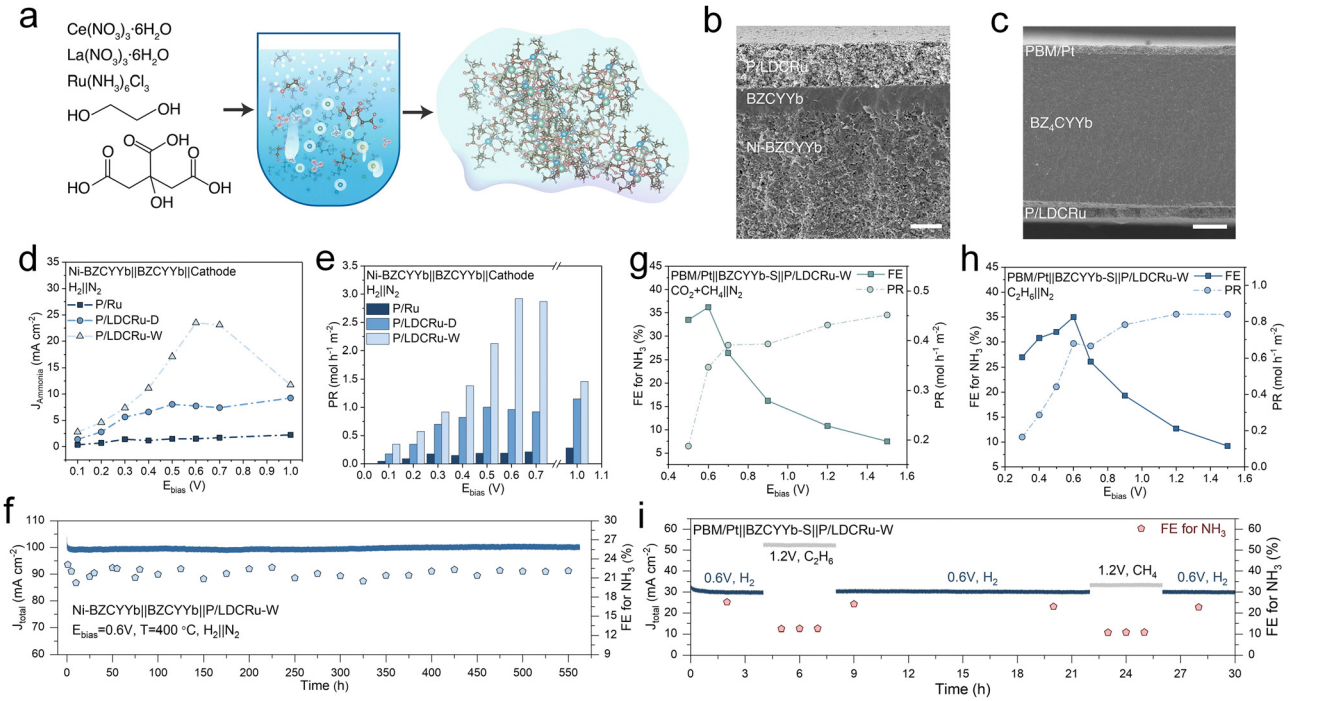

Fig. 6 (a) Schematic of the gel preparation process for the Ru/LDC catalyst. (b) and (c) SEM of two types of PCC for NH_3 production. (d)–(f) Current density, NH_3 production rate, and long term stability of anode support type cells fueled with H_2. (g) FE and production rate of NH_3 with electrolyte support cells with a mixture of CO_2 and CH_4 as fuel. (h) FE and production rate of NH_3 with electrolyte support cells with C_2H_6 as the fuel. (i) Long-term stability of electrolyte support type cell with various fuels. Reproduced with permission.[110] Copyright 2022, Elsevier.

strategies have been explored to enhance the overall performance. Yoo *et al.* attempted NH_3 synthesis using the WOR by introducing both metal electrodes and perovskite-based electrodes (LSCF) into a $BaZr_{0.8}Y_{0.2}O_{3-\delta}$ electrolyte.[126] In their study, an electrolyte-supported cell configuration was employed for the electrochemical synthesis of NH_3 at atmospheric pressure. The feed gas consisted of 3% steam and Ar, supplied to the cell at the operating temperatures ranging from 47 °C to 600 °C. Their results demonstrated that the NH_3 production efficiency varied significantly depending on the catalyst material. Specifically, the Pt electrocatalyst produced less than 10^{-12} mol cm^{-2} s^{-1} of NH_3, while LSCF electrocatalysts showed much higher production rates of 8.5×10^{-11} mol cm^{-2} s^{-1} at 550 °C under 0.8 V. These findings highlight the significantly lower efficiency of steam-based NH_3 synthesis compared to hydrogen-based approaches, necessitating further innovation in material development and system design. To address these challenges, researchers have explored external strategies that can further enhance NH_3 synthesis efficiency in PCECs.

One promising approach is the use of external catalysts integrated into the system to improve reaction kinetics and stability. Sullivan *et al.*, introduced an external Ru-based catalyst to enhance NH_3 production in a PCEC.[113] Fig. 7a–c show a schematic of the PCC with the external catalyst layer integrated into the system. The Ru-based catalyst with high dispersion and uniformity is positioned to facilitate the NH_3 synthesis process. In Fig. 7d, the FE of the cell shows nearly 100% for H_2 between 500 and 1000 mA cm^{-2}. In Fig. 7e, as the driving current density increases from 2000 to 5000 mA cm^{-2}, the NH_3 synthesis rate normalized to the mass of Ru was approximately 2.5×10^{-8} mol cm^{-2} s^{-1} under a current of 5000 mA cm^{-2}. The NH_3 generation rate was quantified using a Drager tube method, enabling direct gas-phase estimation of NH_3 concentration, albeit with lower precision compared to spectroscopic techniques. Despite these improvements, the resulting NH_3 production rates, when normalized to the mass of Ru catalyst, are still comparatively lower than those achieved with other Ru-based catalysts reported in the literature. To address this limitation, the researchers pressurized the NH_3 synthesis reactor up to 12.5 bar by introducing additional hydrogen. This pressurization led to a dramatic increase in NH_3 synthesis rates, reaching as high as 2.1×10^{-6} mol cm^{-2} s^{-1}, which is 100 times higher than the rates achieved under ambient pressure (Fig. 7f). The increased pressure not only enhances reaction kinetics but also shifts the equilibrium to favor NH_3 synthesis, demonstrating the potential of high-pressure conditions for scaling up this technology. A unique aspect of Sullivan *et al.*'s hybrid approach is its capability for cyclic operation, directly enabling transitions between using NH_3 to generate power and using power to synthesize NH_3. Fig. 7g showcased the system's versatility in switching seamlessly between energy generation and NH_3 production modes, making it a promising candidate for practical applications in sustainable energy systems.

Another innovative approach is plasma-assisted NH_3 synthesis. Plasma technology provides a powerful method to activate

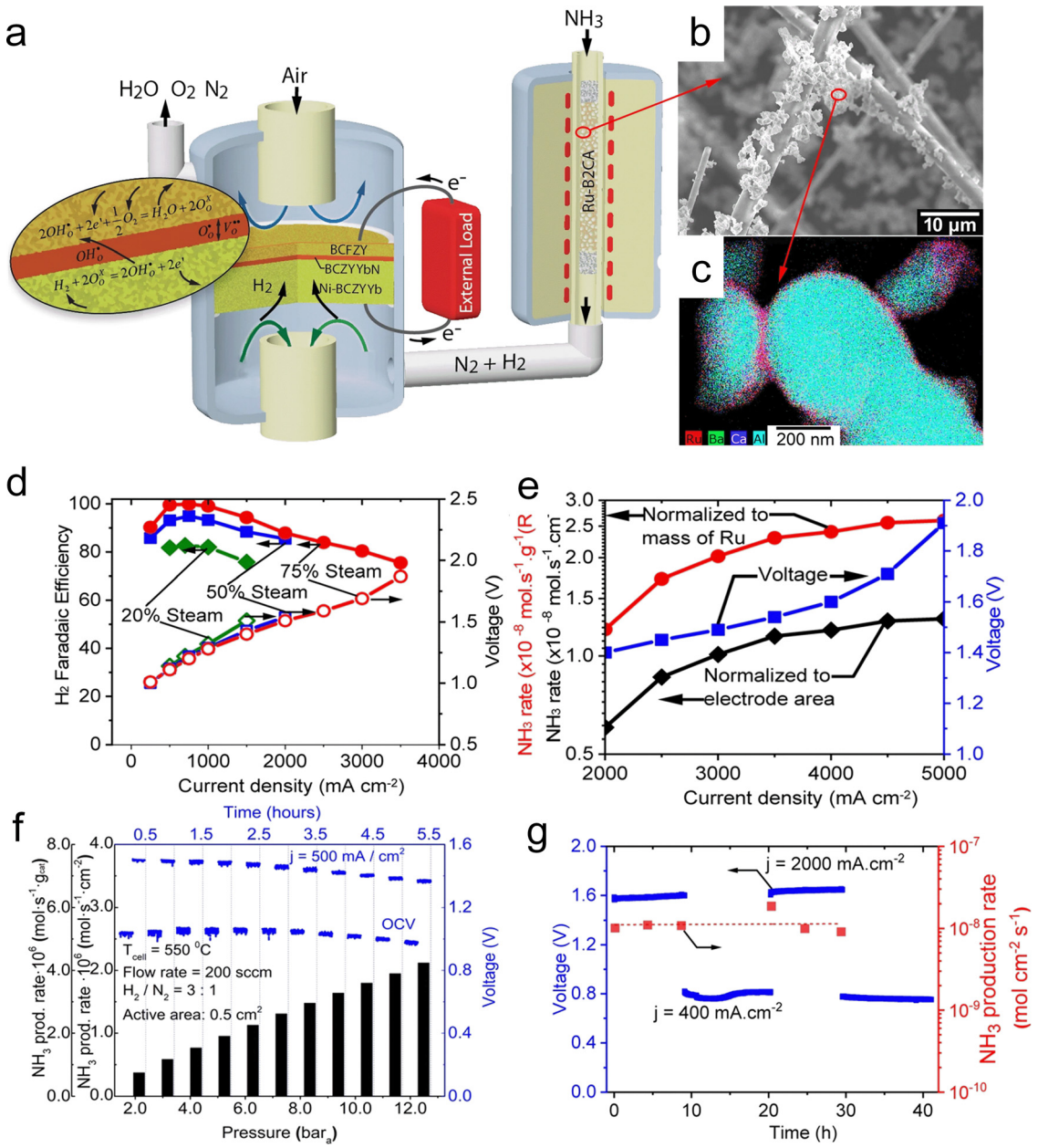

Fig. 7 (a) Schematic for NH_3 production and the power generation process using the Ru–B_2CA catalyst. (b) SEM and (c) TEM image of the Ru–B_2CA catalyst. (d) FE and voltage as a function of the current density of the cell. (e) NH_3 synthesis rate as a function of the current density of the cell. (f) NH_3 synthesis rate as a function of operation pressure. (g) Reversible NH_3 synthesis/NH_3 fuel cell operation result. Reproduced with permission.[113] Copyright 2021, Springer Nature.

N_2 by breaking its triple bond, which is one of the most energy-intensive steps in the NRR. In a study by Sanden *et al.*, a radio frequency (RF) plasma source was applied externally to the PCEC system to aid in N_2 dissociation.[17] The plasma pre-activated N_2 molecules before they reached the cathode, reducing the activation energy required for the NRR. Fig. 8a presents a schematic of the plasma-electrocatalysis setup, showing how the RF plasma is applied to activate nitrogen molecules prior to the electrochemical reaction. The generated NH_3 was diluted with He and then quantified by mass spectrometry. Fig. 8b shows the resulting NH_3 concentration and production rate as a function of the current density, demonstrating the significantly increased NH_3 production rates with plasma activation. Fig. 8c highlights the FE, illustrating that the plasma-assisted process effectively lowers the activation energy for the NRR and improves selectivity. At lower current densities, the plasma-assisted system achieves a FE of up to 88%, though this efficiency decreases as current density increases due to the competing HER reaction. These additional techniques offer new pathways for overcoming the inherent limitations of steam-based NH_3 synthesis *via* the WOR. By addressing the challenges of electrode performance, nitrogen activation, and

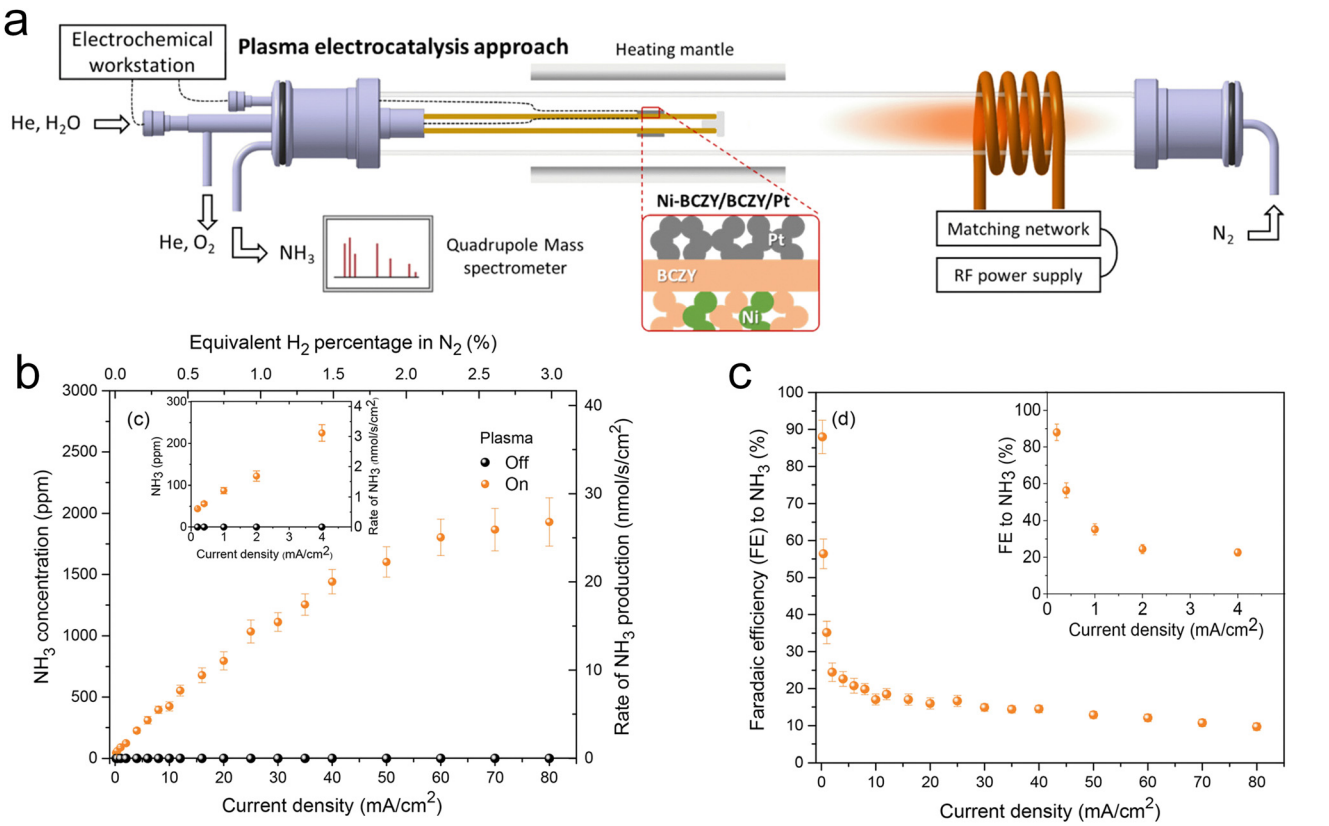

Fig. 8 (a) Schematic representation of the hybrid plasma electrochemical reactor setup. (b) NH_3 production rate as a function of current density and (c) faradaic efficiency of NH_3 production with/without 80 W plasma power. Reproduced with permission.[17] Copyright 2020, American Chemical Society.

overall system efficiency, these innovative approaches bring NH_3 synthesis in PCECs closer to being a competitive alternative to traditional methods.

4.2. Direct NH_3 utilization in PCFCs

Unlike NH_3 synthesis, NH_3 decomposition is an endothermic reaction ($2NH_3 \rightarrow 3H_2 + N_2$, $\Delta H = +45.9$ kJ mol^{-1}). By reducing the flow rate of the reactant gas mixture, the residence time of NH_3 molecules on the catalyst surface is extended, allowing for more opportunities for reaction. Consequently, elevated operating temperatures and decreased flow rates can promote NH_3 decomposition.[102,131] The overall performance of DA-PCFCs is strongly dependent on the rate at which NH_3 is decomposed at the anode, highlighting the crucial role of anode catalysis in these systems. The NH_3 decomposition rate increases with NH_3 partial pressure and decreases with H_2 partial pressure, which can be described by the Temkin–Pyzhev equation:[132,133]

$$\gamma = k\left(\frac{P_{NH_3}^2}{P_{H_2}^3}\right)^{0.25} \quad (1)$$

Additionally, the materials and thicknesses of the anode, electrolyte, and cathode significantly impact the overall performance of DA-PCFCs.[4,134,135] Therefore, the recent research on DA-PCFCs will be described from the aspects of anodes, electrolytes, and cathodes.

4.2.1. Anodes. In DA-PCFCs, NH_3 molecules are initially adsorbed onto the anode surface, where they undergo decomposition to form N_2 and H_2. Subsequently, the generated H_2 undergoes electrochemical oxidation.[136,137] Consequently, the anode's catalytic activity for NH_3 decomposition is paramount to the cell's performance. Common anode materials in DA-PCFCs primarily consist of Ni-based ceramics and Pd-based materials, including Ni–$BaZr_{0.1}Ce_{0.7}Y_{0.2}O_{3-\delta}$ (Ni–BZCY), Ni–$BaZr_{0.1}Ce_{0.7}Y_{0.1}Yb_{0.1}O_{3-\delta}$ (Ni–BZCYYb), and Pd.

Among single-metal catalysts, Ru-based catalysts exhibit the high activity and stability for NH_3 decomposition, as depicted in Fig. 9a.[138,139] Masel *et al.* identified N_2 desorption as the rate-determining step (RDS) in NH_3 decomposition over Fe, Co, and Ni surfaces, while the cleavage of N–H bonds is the RDS on Rh, Ir, Pd, Pt, and Cu surfaces. They also experimentally determined the following activity order: Ru > Ni > Rh > Co > Ir > Fe > > Pt > Cr > Pd > Cu ≫ Te, Se, Pb.[140] Although Ru offers superior catalytic activity to Ni, its high cost and scarcity have hindered its widespread application. Therefore, Ni was extensively investigated as a potential catalyst for NH_3 decomposition. Furthermore, the excellent electronic conductivity of Ni is beneficial for enhancing the NH_3 decomposition process (Fig. 9b).[141] Therefore, Ni has been the focus of extensive research as an NH_3 decomposition catalyst.

In 2015, Yang *et al.* introduced Ni–$BaCe_{0.75}Y_{0.25}O_{3-\delta}$ (Ni–BCY25) as a promising anode for DA-PCFCs.[142] Notably,

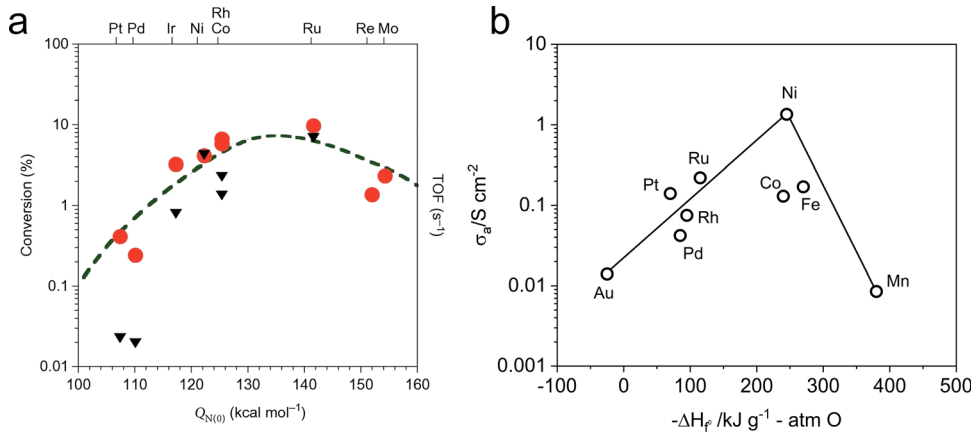

Fig. 9 (a) Relationship of theoretical NH_3 decomposition volcano curve and experimental turnover frequencies (TOFs) of various transition-metal catalysts at 850 K obtained by microkinetic modeling and the nitrogen binding energies ($Q_{N(0)}$). Reproduced with permission.[138] Copyright 2021, American Chemical Society. (b) The relationship diagram between anodic polarization conductivity of various metals at 1000 °C and heat of oxide generation function. Reproduced with permission.[141] Copyright 2024, Wiley-VCH.

the NH_3 decomposition rate of Ni–BCY25 at temperatures ranging from 400 to 700 °C significantly surpassed those of Ni–8mol% Y_2O_3–ZrO_2 and Ni–$Ce_{0.90}Gd_{0.10}O_{1.95}$ (Fig. 10a). They further investigated the impact of steam content on NH_3 decomposition over the Ni–BCY25 anode, as depicted in Fig. 10b. Introducing 0.8% steam led to a significant decline in the NH_3 decomposition rate. This reduction primarily stems from steam adsorption onto the BCY25 surface. The resulting species, including hydroxide groups and protons, can potentially occupy active reaction sites at the interface between the nickel catalyst and the BCY25 support, resulting in a significant water poisoning effect.[143,144] When operating on NH_3 fuel, a promising peak power density (PPD) of 216 mW cm^{-2} was attained at 650 °C in a single cell designated as Ni–BCY25|$BaCe_{0.9}Y_{0.1}O_{3-\delta}$|$Sm_{0.5}Sr_{0.5}CoO_{3-\delta}$ (Fig. 10c). Miyazaki *et al.* assessed the suitability of Ni–$Ba(Zr,Y)O_{3-\delta}$ (Ni–BZY) as DA-PCFC anodes by comparing the NH_3 decomposition activity of Ni–BZY10, Ni–BZY20, Ni–BCY10, and Ni–YSZ.[145] As depicted in Fig. 10d, Ni–BZY10 and Ni–BZY20 catalysts exhibited superior NH_3 decomposition performance compared to Ni–YSZ, suggesting that proton conductors play a more significant role in the decomposition process. Among the catalysts evaluated

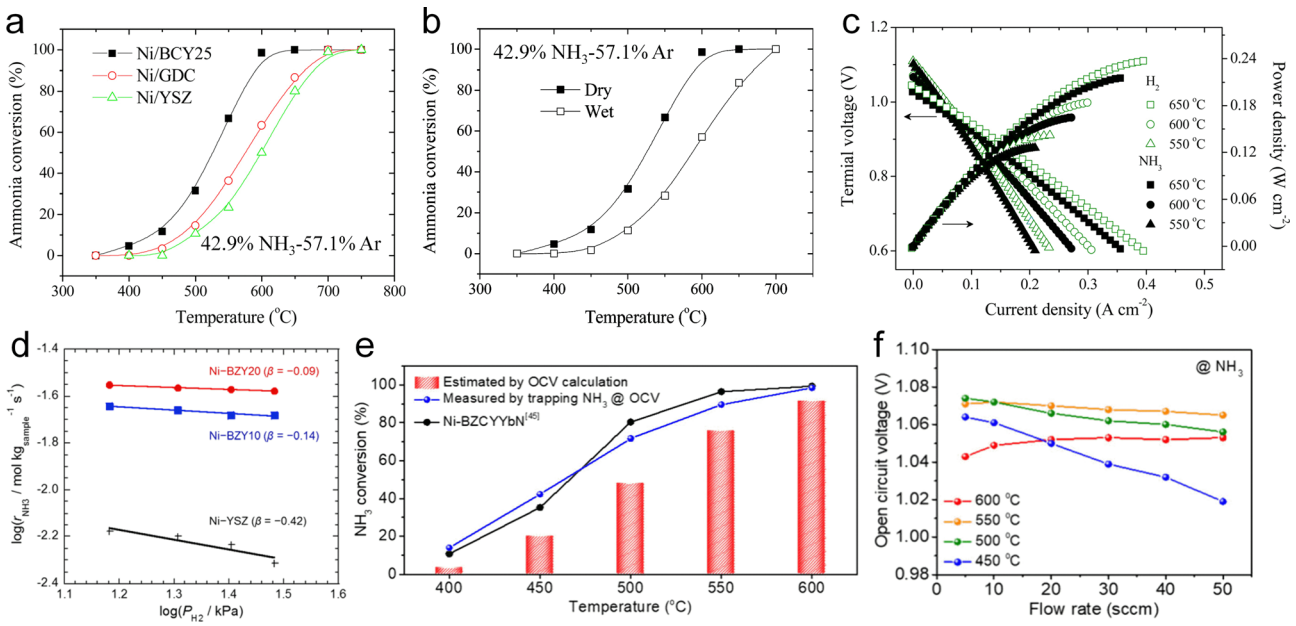

Fig. 10 (a) NH_3 conversion on several Ni-based anodes. (b) NH_3 conversion on Ni–BCY25 in dry and wet gases. (c) *I–V–P* curves of a cell with the structure of Ni–BCY25|BCY10|SSC. Reproduced with permission.[142] Copyright 2015, American Chemical Society. (d) NH_3 decomposition rate as a function of partial pressure of hydrogen on several Ni-based anodes at 500 °C. Reproduced with permission.[145] Copyright 2017, Elsevier. (e) NH_3 conversion rate of the Ni–BCZYYb4411 anode on a PCFC. (f) OCV as functions of NH_3 flow rate from 450 to 600 °C. Reproduced with permission.[146] Copyright 2024, American Chemical Society.

for NH_3 decomposition under varying H_2 partial pressures, Ni–BZY20 exhibited the highest NH_3 conversion activity and resistance to hydrogen inhibition. Additionally, a DA-PCFC comprising a Ni–BZY20 anode, a BZY20 electrolyte, and a Pt cathode achieved a PPD of 125 mW cm^{-2} at 700 °C. The study by Haile *et al.* using Ni–BZCYYb4411 as the anode in a DA-PCFC revealed a strong correlation between NH_3 conversion rate and open circuit voltage.[146] While NH_3 conversion rates above 85% were achieved at temperatures above 550 °C (Fig. 10e), a substantial decrease to 40% was observed at 450 °C, likely explaining the sharp OCV reduction at this temperature (Fig. 10f). A further observation was the rapid decrease in OCV with increasing NH_3 flow rate, suggesting that higher flow rates hinder NH_3 decomposition and consequently affect the cell performance. The Ni component within the Ni-based ceramic anode of DA-PCFCs is susceptible to the formation of Ni_3N when exposed to NH_3. However, Ni_3N can be readily reduced by hydrogen, leading to structural degradation of the anode and compromising the long-term stability of DA-PCFCs.[11,105,147] The strong chemisorption of nitrogen atoms onto Ni-based catalysts, while promoting NH_3 decomposition, can also hinder N_2 desorption, resulting in a poisoning effect and limiting the overall NH_3 decomposition rate.[141,148]

The catalytic activity of Ni-based ceramic anodes for NH_3 decomposition can be enhanced by the *in situ* exsolution of B-site cations. Shao *et al.* proposed a Pd-doped perovskite BZCYYb (BZCYYbPd) and evaluated its NH_3 decomposition activity as a DA-PCFC anode (Fig. 11a–e).[149] As indicated in Fig. 11b and c, Pd metal nanoparticles exsolved from the BZCYYbPd lattice, creating B-site deficient structures that facilitate proton conduction.[150] Fig. 10d demonstrates that Ni–BZCYYbPd exhibits superior NH_3 decomposition activity compared with Ni–BZCYYb, primarily attributed to the beneficial effects of Pd nanoparticles and B-site defect structures. Therefore, the Ni–BZCYYbPd anode enabled the DA-PCFC to achieve a PPD of 724 mW cm^{-2} at 650 °C (Fig. 11e). They also developed a Ru and Fe co-doped PCFC anode material, Ni–$Ba(Zr_{0.1}Ce_{0.7}Y_{0.1}Yb_{0.1})_{0.94}Ru_{0.03}Fe_{0.03}O_{3-\delta}$.[135] Secondary oxidation–reduction treatment led to the formation of more RuFe nanoparticles on the surface, enhancing its catalytic activity for NH_3 decomposition. Consequently, the electrochemical performance of the DA-PCFC with this anode was significantly improved. Recently, Ciucci *et al.* developed a novel DA-PCFC anode denoted as Ni–$Ba(Zr_{0.1}Ce_{0.7}Y_{0.1}Yb_{0.1})_{0.95}Ni_{0.05}O_{3-\delta}$ (BZCYYbNi), which significantly improved the electrochemical performance of DA-PCFCs.[151] Ni nanoparticles exsolved from the BZCYYbNi perovskite structure create numerous active sites for NH_3 decomposition, significantly boosting the catalytic activity of the Ni–BZCYYbNi anode (Fig. 11f). A DA-PCFC employing the Ni–BZCYYbNi ceramic anode achieved a PPD of 523 mW cm^{-2} at 650 °C, as illustrated in Fig. 11g. The Ni–BZCYYbNi anode offers a more cost-effective alternative to Pd-based anodes for DA-PCFCs due to the lower cost of Ni.

Incorporating high catalytic activity species (Ru, Fe, *etc.*) into Ni-based anodes can significantly enhance DA-PCFCs' performance and operating stability. Chen *et al.* successfully developed high-performance DA-PCFCs by decorating Ni–BZCYYb anodes with Fe, achieving a PPD of 1.257 W cm^{-2} at 650 °C.[152] Fe modification alters the adsorption strength of NH_3 and the barrier for N_2 associative desorption, contributing to improved performance and stability. In their another study, they infiltrated $Ru_{0.95}Cu_{0.05}$ into the Ni–BZCYYb anode, resulting in the formation of $Ru_{0.95}Cu_{0.05}Ni_x$ (RCN) catalysts through an *in situ* reaction between $Ru_{0.95}Cu_{0.05}$ nanoparticles and Ni grains (Fig. 12a and b).[99] As shown in Fig. 12c, the RCN–BZCYYb anode exhibited the highest NH_3 decomposition rate among the evaluated anodes (~98% at 550 °C). Consequently, DA-PCFCs with RCN-catalyzed Ni–BZCYYb anodes demonstrated a high PPD of 732 mW cm^{-2} and enhanced stability. Recently, Shim *et al.* treated a Ni–BZCYYb anode with a Pd catalyst using atomic layer deposition (ALD).[153] This process formed a Pd catalytic layer on the Ni–BZCYYb surface and introduced some Pd atoms into the anode's interior (Fig. 12d). This approach effectively improved NH_3 decomposition rates, inhibited Ni_3N formation, and enhanced DA-PCFC performance and durability (Fig. 12e).

4.2.2. Electrolytes. In DA-PCFCs, hydrogen protons, generated through NH_3 decomposition and H_2 oxidation, traverse the electrolyte to react with oxygen species. Consequently, an exceptionally thin-film electrolyte can significantly reduce ohmic resistance and enhance proton conduction, leading to improved DA-PCFC performance at lower temperatures. $BaCeO_{3-\delta}$ based oxides are often employed as the electrolytes of DA-PCFCs, such as $BaCe_{0.8}Gd_{0.2}O_{2.9}$ (BCG),[154,155] $BaCe_{0.9}Nd_{0.1}O_{3-\delta}$ (BCN),[156] $BaCe_{0.8}Gd_{0.19}Pr_{0.01}O_{3-\delta}$ (BCGP),[157] $BaCe_{0.8}Y_{0.2}O_{3-\delta}$ (BCY),[158,159] $BaCe_{0.8}Sm_{0.2}O_{3-\delta}$ (BCS),[160] $BaZr_{0.1}Ce_{0.7}Y_{0.2}O_{3-\delta}$ (BZCY)[161] and $BaZr_{0.1}Ce_{0.7}Y_{0.1}YbO_{3-\delta}$ (BZCYYb).[99,152] Various techniques exist for fabricating thin-film electrolytes for DA-PCFCs, including wet colloidal spraying,[162] modified suspension spraying,[160] radio frequency (RF) sputtering deposition[163] and tape casting.[99] Maffei *et al.* successfully deposited a 15 μm thin-film BCY electrolyte onto a NiO-BCY anode using wet colloidal spraying.[162] Habazaki *et al.* employed RF sputtering to fabricate a 1 μm-thick BZCY electrolyte film on a Pd solid anode, achieving a PPD of 0.58 W cm^{-2} at 600 °C.[164] However, the high cost of Pd may impede its widespread adoption. Recently, Duan *et al.* introduced ultrasonic spray coating for thin-film electrolyte fabrication, controlling electrolyte thickness at 3 μm, thereby minimizing proton transport resistance across grain boundaries and effectively reducing the cells' ohmic impedance (Fig. 13a).[165] Co-tape casting and co-sintering, a technology enabling precise control of electrolyte thickness, has also gained attention in DA-PCFCs. Liu *et al.* introduced the detailed co-tape casting and co-sintering process (Fig. 13b) and fabricated DA-PCFCs with ~10 nm electrolyte.[99] These DA-PCFCs showed high performance and remarkable durability, which indicates that the co-tape casting and co-sintering technology has significant promise for DA-PCFC development.

4.2.3. Cathodes. In DA-PCFCs, cathodes exhibiting superior triple conducting behavior ($e^-/O^{2-}/H^+$) can substantially enhance the cell performance. Given that the distinction

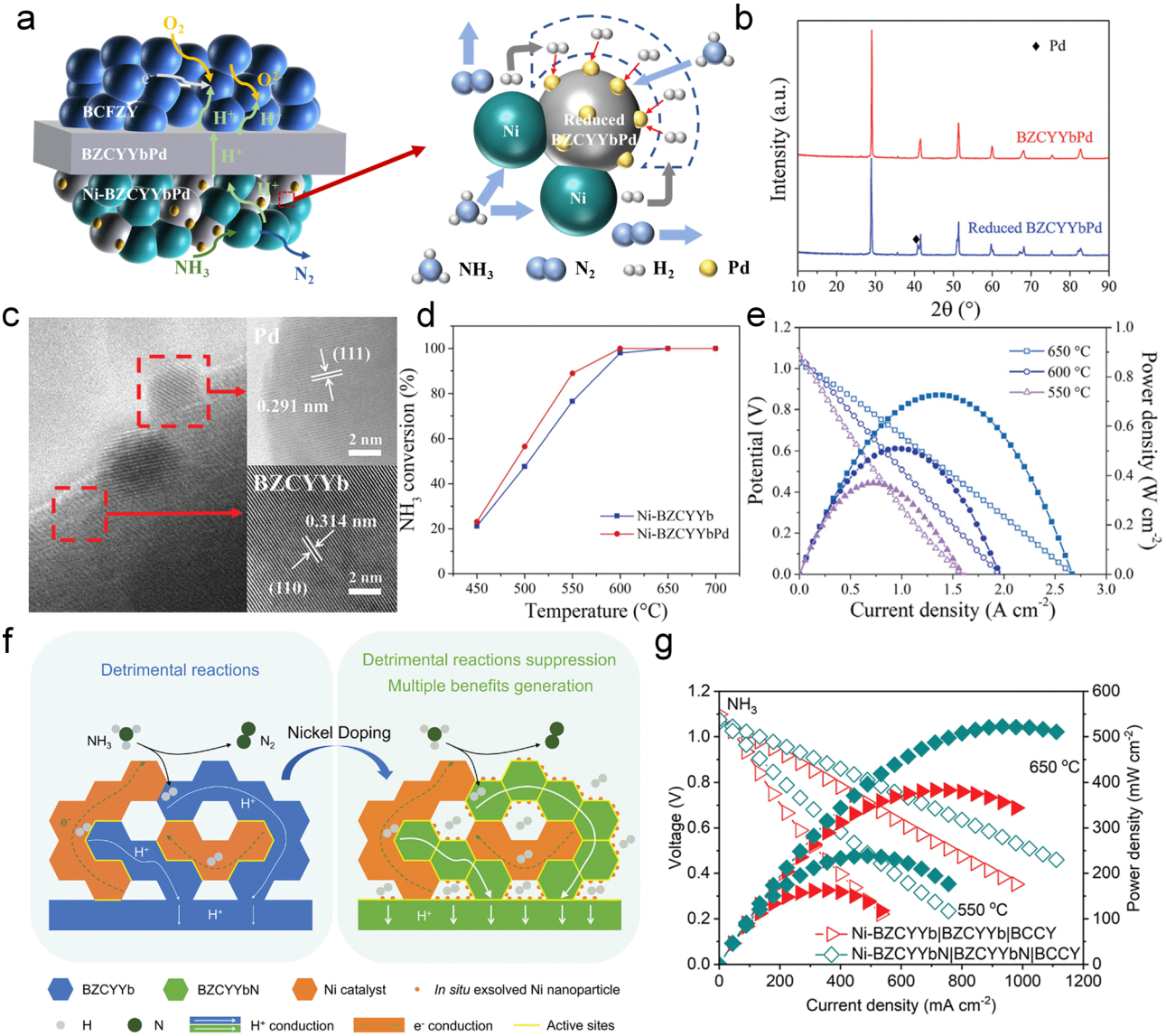

Fig. 11 (a) The operating mechanism of DA-PCFCs with the Ni–BZCYYbPd anode and NH_3 decomposition pathway on the Ni–BZCYYbPd anode. (b) XRD patterns and (c) HR-TEM images of BZCYYbPd powder before and after H_2 reduction at 650 °C. (d) NH_3 conversion rates of Ni–BZCYYb and Ni–BZCYYbPd. (e) *I–V–P* curves of the DA-PCFC. Reproduced with permission.[149] Copyright 2021, Wiley-VCH. (f) Schematic of DA-PCFCs: (left) Ni–BZCYYb anode and BZCYYb electrolyte; (right) Ni–BZCYYbNi anode and BZCYYbNi electrolyte. (g) *I–V–P* curves of a DA-PCFC with the Ni–BZCYYbNi anode. Reproduced with permission.[151] Copyright 2022, Wiley-VCH.

between H_2-fueled PCFC lies in the fuel gas, H_2-fueled PCFC cathodes can also be utilized in DA-PCFCs. Consequently, we will outline some recent research on H_2-fueled PCFC cathodes.

O'Hayre *et al.* demonstrated a high-performance PCFC cathode by infiltrating the triple conductor $BaCo_{0.4}Fe_{0.4}Zr_{0.1}Y_{0.1}O_{3-\delta}$ (BCFZY) into a $BaZr_{0.3}Ce_{0.6}Y_{0.1}O_{3-\delta}$ (BZCY63) framework (Fig. 14a).[97] The high oxygen vacancy concentration and proton conductivity of BCFZY contribute to its superior catalytic activity,[166] enabled the corresponding PCFC to achieve a PPD of 0.648 W cm^{-2} at 600 °C (Fig. 14b) and maintain stable operation for over 1100 h at 500 °C (Fig. 14c). Some high-performance BCFZY derivatives were further developed, such as $Ba_{0.9}Co_{0.4}Fe_{0.4}Zr_{0.1}Y_{0.1}O_{3-\delta}$,[167] $BaCo_{0.7}Fe_{0.1}Zr_{0.1}Y_{0.1}O_{3-\delta}$,[168] $Ba(Co_{0.4}Fe_{0.4}Zr_{0.1}Y_{0.1})_{0.95}Ni_{0.05}O_{3-\delta}$,[169] BCFZY–NiO,[170] $Ba(Co_{0.4}Fe_{0.4}Zr_{0.1}Y_{0.1})_{0.95}Mg_{0.05}O_{3-\delta}$[32] and $Ba_{0.95}(Co_{0.4}Fe_{0.4}Zr_{0.1}Y_{0.1})_{0.95}Ni_{0.05}O_{3-\delta}$,[171] which can also be applied to DA-PCFCs.

Shao *et al.* developed a PCFC triple-conducting nanocomposite cathode $BaCo_{0.7}(Ce_{0.8}Y_{0.2})_{0.3}O_3$ (BCCY), comprising $BaCe_{0.8}Y_{0.2}O_3$ (P-BCCY) as a proton conductor, $BaCo_{0.9}(Ce_{0.8}Y_{0.2})_{0.1}O_3$ (M-BCCY) as an oxygen-ion conductor, and $BaCoO_{3-\delta}$ (BC) with high electronic conductivity (Fig. 15a–c).[172] This synergistic combination endowed BCCY with excellent catalytic activity. When employed as a PCFC cathode, BCCY achieved a high PPD of 508 mW cm^{-2} at 550 °C and demonstrated an operational stability exceeding 800 h (Fig. 15d and e).

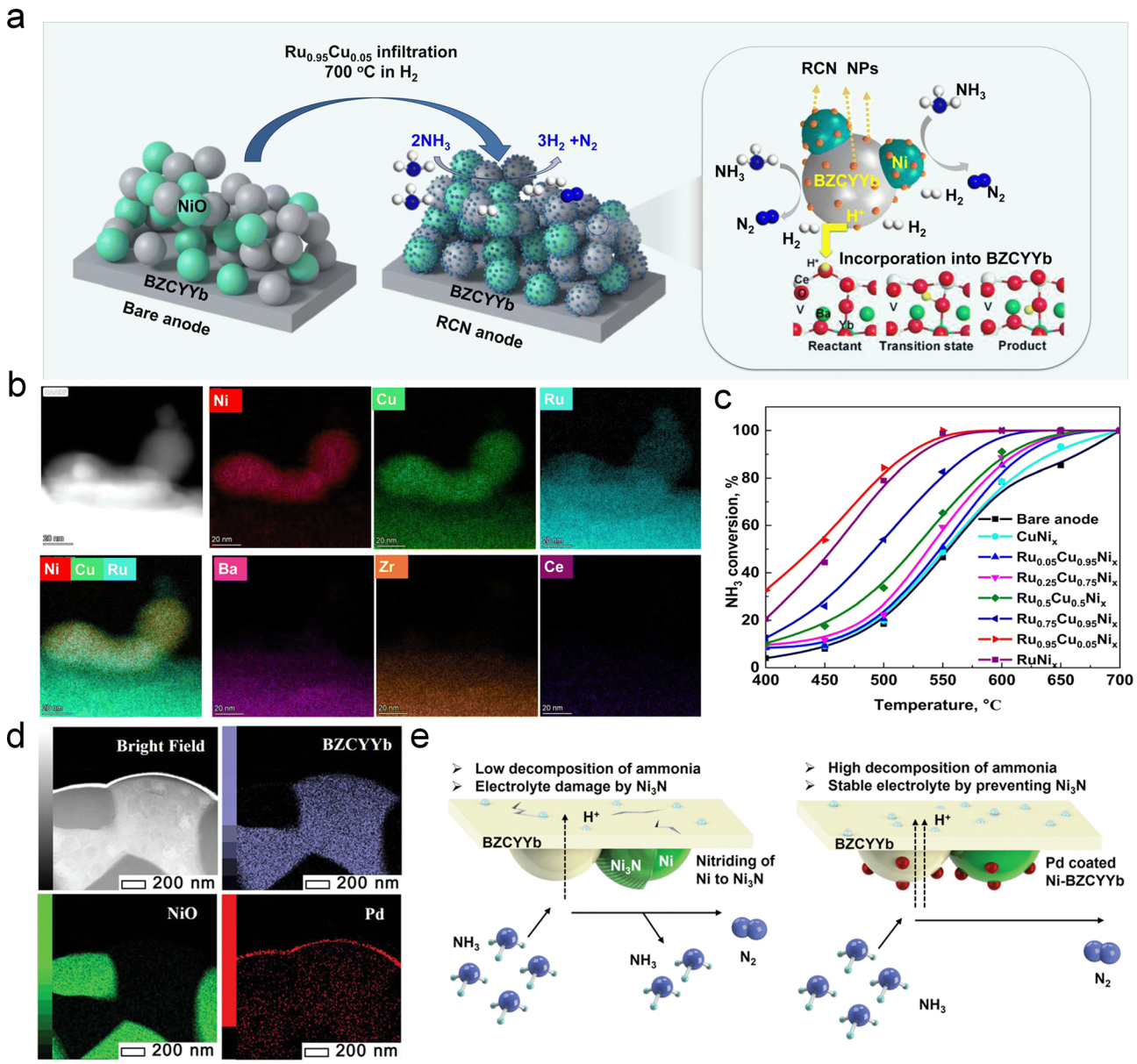

Fig. 12 (a) Schematic illustration of NH_3 decomposition on the RCN nanoparticle-modified Ni–BZCYYb anode. (b) STEM-EDX mapping results of the RCN–Ni–BZCYYb anode. (c) NH_3 decomposition rates of Ni–BZCYYb and Ru_xCu_{1-x}–Ni/BZCYYb (x = 0–1) anodes. Reproduced with permission.[152] Copyright 2022, Royal Society of Chemistry. (d) Bright-field, BZCYYb, NiO, and Pd TEM-EDS mapping images. (e) Schematic illustration of the nitridation of Ni in bare Ni–BZCYYb (left) and Pd-treated Ni–BZCYYb (right) anodes of DA-PCFCs. Reproduced with permission.[153] Copyright 2023, Wiley-VCH.

4.2.4. External NH_3 cracking reactor and anode catalytic layer. While Ni catalysts demonstrate reasonable catalytic activity for NH_3 decomposition, prolonged exposure to high-concentration NH_3 under operating conditions can lead to Ni phase coarsening, agglomeration, and nitridation, ultimately causing significant cell degradation. To mitigate this issue, Sullivan *et al.* coupled an NH_3-cracking reactor containing the Ru–$(BaO)_2(CaO)(Al_2O_3)$ (Ru–B_2CA) catalyst to DA-PCFCs.[113] The Ru–B_2CA catalyst, supported on refractory insulating fibers, exhibits high catalytic activity for NH_3 decomposition, enabling a PPD of 0.65 W cm^{-2} and stability of 1250 h for DA-PCFCs at 600 °C.

Incorporating an anode catalytic layer (ACL) can also effectively enhance both the performance and durability of DA-PCFCs. Liu *et al.* fabricated tubular DA-PCFCs featuring an iron catalytic layer on the Ni–BZCYYb anode (Fig. 16a).[173] These DA-PCFCs, utilizing a highly active Fe catalyst for NH_3 decomposition, achieved a record PPD of 1.078 W cm^{-2} at 700 °C for tubular DA-PCFCs. By decomposing most of the NH_3 into H_2 and N_2, the Fe catalytic layer minimizes direct contact between NH_3 and the Ni–BZCYYb anode, thus enhancing the stability of the tubular DA-PCFCs. The high catalytic activity of Fe for NH_3 decomposition has also been demonstrated in other studies.[106,174] Chen *et al.* prepared a material designated as

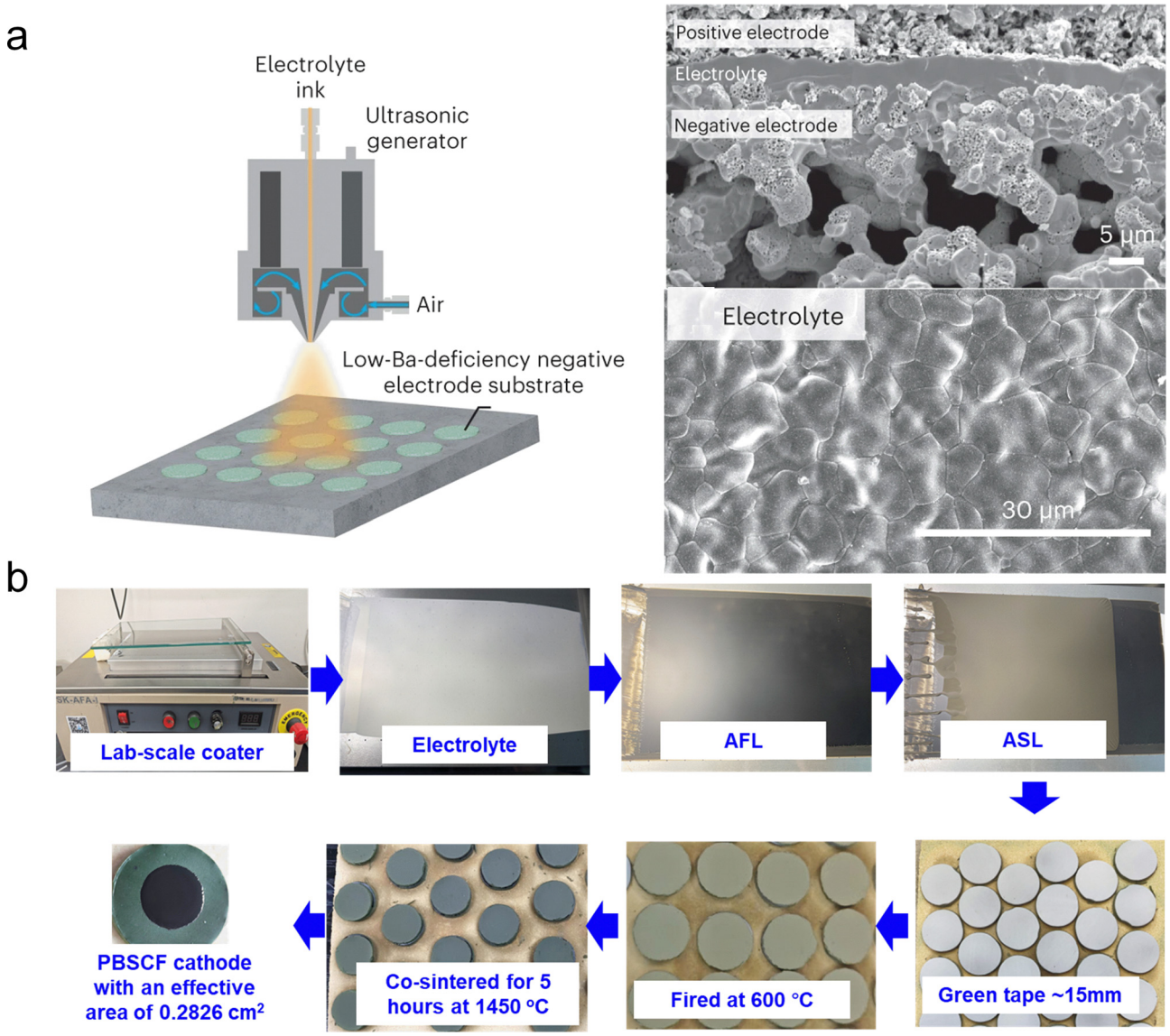

Fig. 13 (a) The ultrasonic spray coating process for preparing thin-film electrolytes and SEM images of the single cell. Reproduced with permission.[165] Copyright 2023, Nature Portfolio. (b) Fabrication process of the single cell using a tape casting technique. Reproduced with permission.[152] Copyright 2022, Royal Society of Chemistry.

Fe–CeO_x (Fe : Ce = 6 : 4) *via* a wet chemical method and incorporated it as a catalytic layer on the anode side of DA-PCFCs (Fig. 16b).[175] This composite material not only maintains a high NH_3 decomposition rate but also suppresses the formation of iron nitride, ensuring the long-term operational stability of DA-PCFCs.

Beyond simple metal catalytic layers, perovskite oxides present an alternative for the DA-PCFC catalytic layer, enhancing cell performance and stability. In 2023, Chen *et al.* developed the reduced $Sr_2Fe_{1.35}Mo_{0.45}Cu_{0.2}O_{6-\delta}$ (r-SFMC) anode catalytic layer, which demonstrates high NH_3 adsorption and decomposition capabilities (Fig. 17a and b).[176] The tubular Ni–BZCYYb anode-supported DA-PCFCs equipped with an r-SFMC ACL achieved a remarkable PPD of 1.02 W cm^{-2} and exhibited outstanding stability over 200 h at 650 °C, marking a significant advancement in DA-PCFC technology (Fig. 17c). More recently, Shao *et al.* substituted 5, 10, 15 and 20% Ru into $Pr_{0.6}Sr_{0.4}Co_{0.2}Fe_{0.8}O_{3-\delta}$ (PSCF), respectively, and found reduced-$Pr_{0.6}Sr_{0.4}(Co_{0.2}Fe_{0.8})_{0.85}Ru_{0.15}O_{3-\delta}$ (r-PSCFR15) exhibits the optimal NH_3 decomposition activity among these catalysts (Fig. 17d).[100] During the reduction process, CoFe (CF) and CoFeRu (CFR) alloys form on the PSCF and PSCFR15 surfaces, respectively. The CFR alloy promotes the N_2 desorption process in the NH_3 decomposition reaction, thereby boosting NH_3 decomposition efficiency (Fig. 17e and f). Under the influence of the r-PSCFR15 catalytic layer, the DA-PCFC exhibited a significant improvement in cell performance, reaching 625 mW cm^{-2} at 650 °C. Additionally, the DA-PCFC demonstrated robust durability, maintaining stable performance over 340 h (Fig. 17g). After the operational stability test, the Ni

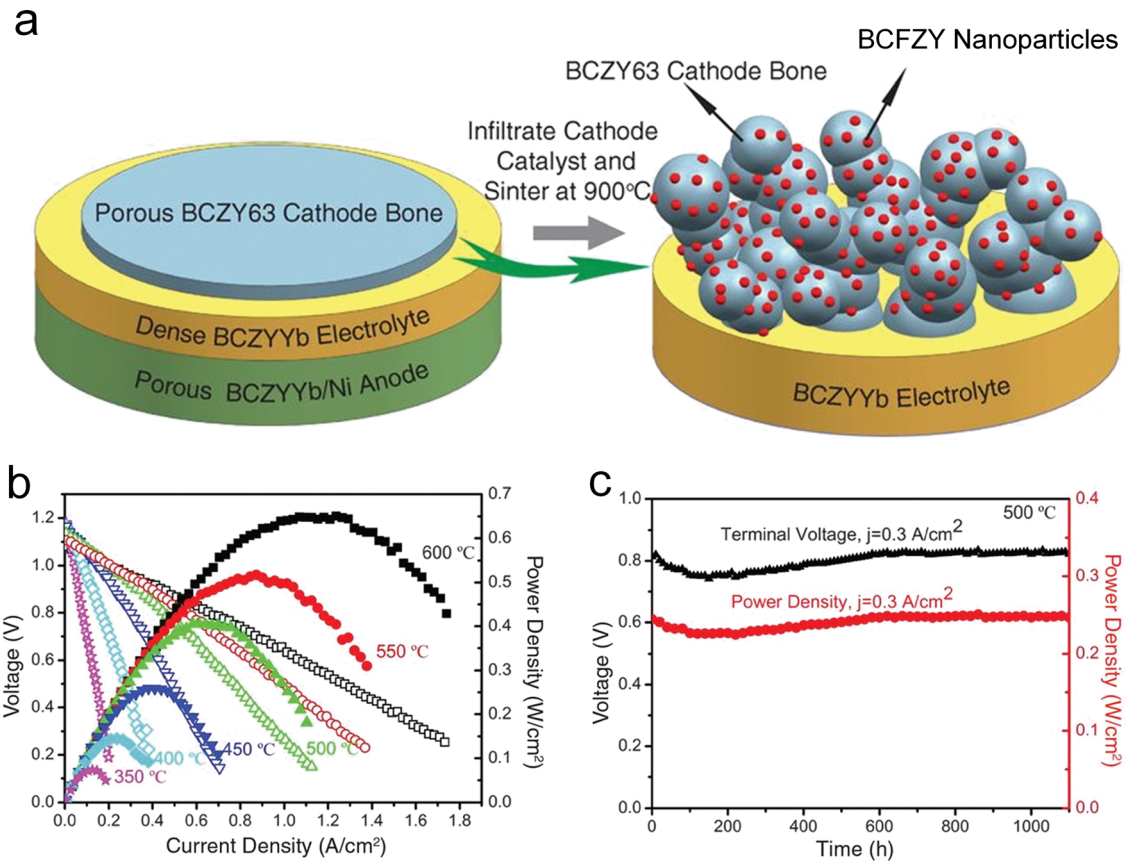

Fig. 14 (a) Process for preparing BCFZY infiltrated BCZY63 composite. (b) *I*–*V*–*P* and (c) stability of the cells under H_2/air. Reproduced with permission.[97] Copyright 2015, American Association for the Advancement of Science.

particles in the anode of the PCFC with r-PSCFR15 ACL were noticeably smaller compared to those on the anodes without ACL (Fig. 17h and i), which indicates that the r-PSCFR15 effectively prevented the Ni sintering in the Ni-based anode.

5. Perspectives for electricity-to-NH_3 interconversion in PCCs

5.1. NH_3 synthesis in PCECs

The low FE and NH_3 production rate in PCEC NH_3 synthesis are primarily attributed to the competitive HER.[88] To enhance these metrics, future research should prioritize the development of catalysts with high NRR activity. Optimizing the electronic structure, crystal structure, and surface morphology of catalysts can effectively suppress the HER and promote the NRR. Exploring novel catalytic materials, such as nitride catalysts, is also crucial. DFT calculations and advanced *in situ* characterization techniques can aid in identifying the active sites for the HER and NRR, significantly benefiting the development of NH_3 synthesis catalysts. Moreover, optimizing electrolyte design and NH_3 synthesis operating conditions is of paramount importance.

5.1.1. Investigations of nitride-based electrodes. Nitride-based catalysts, with their unique electronic and structural properties, have garnered significant interest in the field of NH_3 synthesis.[177–180] Their nitrogen vacancies can enhance the reactivity and selectivity of the NRR, making them promising alternatives to precious metal catalysts. In addition to lower cost, nitrides offer considerable potential for NH_3 synthesis. A comprehensive understanding of nitride behavior under PCEC operating conditions is crucial for their successful implementation. This necessitates further investigation into their long-term stability and performance under high temperatures, mixed N_2/H_2 environments, and electrical biases. Examining the long-term stability of nitride electrodes under operating conditions is a crucial area for future research.

5.1.2. Identification of NRR and HER active sites. Currently, the FE of PCEC NH_3 synthesis remains low, primarily due to the competitive relationship between the HER and the NRR at the PCEC cathode. A deeper understanding of catalyst properties can enable better optimization of NRR activity and NH_3 selectivity. If the active sites for NRR and HER can be identified through density functional theory (DFT) calculations and *in situ* characteristics (*in situ* XPS or Raman), catalysts can be optimized to increase NRR active sites and reduce HER active sites, thereby maximizing the FE of PCEC NH_3 synthesis.[181,182] However, PCEC NH_3 synthesis technology is still in its nascent stage, resulting in a scarcity of reports on NRR active sites at the atomic scale. Additionally, screening for

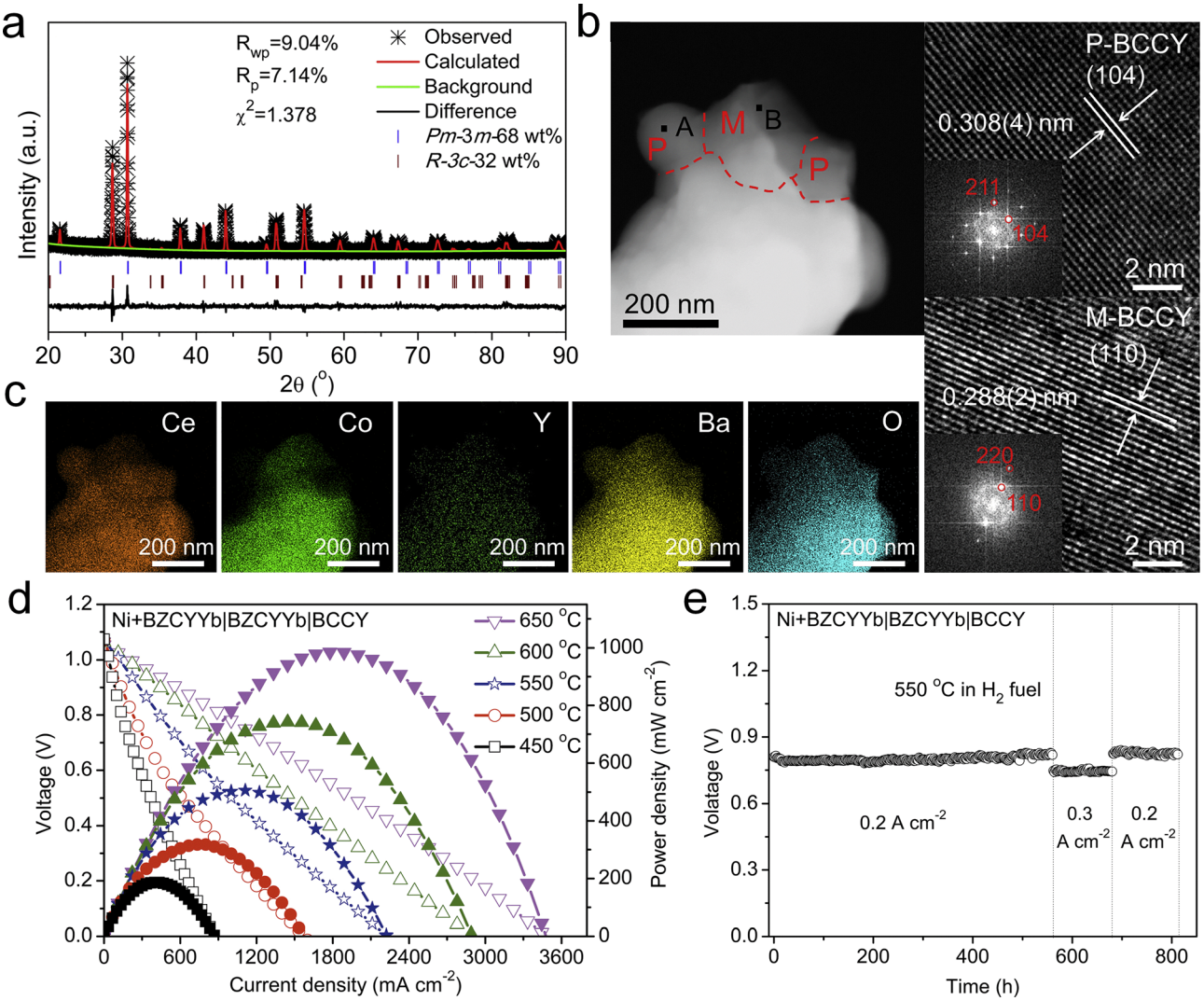

Fig. 15 (a) Refined XRD profiles of the BCCY sample. (b) STEM image and (c) STEM-EDX result of BCCY. (d) *I*–*V*–*P* curves and (e) durability of PCFCs with the BCCY cathode. Reproduced with permission.[172] Copyright 2019, Cell Press.

the optimal catalyst model within a given catalyst system through DFT calculations, followed by experimental validation, could significantly expedite progress in this field.

5.1.3. Investigations of electrolyte materials and structures. In PCECs, the choice of electrolyte plays a crucial role in determining the overall performance of the cell, as electronic leakage in protonic conducting electrolytes can significantly reduce FE. Promising proton conducting electrolytes such as BZCYYb4411 and BZCYYb7111 exhibit mixed ionic-electronic conductivity at elevated temperatures.[5,56] At 600 °C, the electronic transport number of BZCYYb7111 is approximately 0.1, indicating that a portion of the applied current is lost through electronic leakage rather than being utilized for electrochemical reactions. This electronic leakage can significantly reduce FE, particularly in PCEC modes (including electrochemical NH_3 synthesis). Strategies to mitigate this issue and enhance overall efficiency include optimizing electrolyte composition, reducing operating temperatures, employing moderate current densities, and enhancing the catalytic activity of electrodes.

5.1.4. Operation condition optimization. NH_3 synthesis in PCECs can benefit from optimizing operating conditions, especially regarding pressure and temperature. Studies, such as those involving Ru-based external catalysts, have shown significant increases in NH_3 production rates at higher pressures.[113] Operating PCECs under elevated pressures can shift reaction equilibria favorably toward NH_3 synthesis. Therefore, exploring advanced materials capable of withstanding high-pressure environments and conducting systematic studies on temperature-pressure combinations could lead to enhanced NH_3 production rates while ensuring long-term stability.

5.2. Direct NH_3 utilization in PCFCs

5.2.1. NH_3 decomposition rate at low temperatures. In DA-PCFCs, NH_3 undergoes initial decomposition into H_2 and N_2 on anodes, with the generated H_2 subsequently participating in

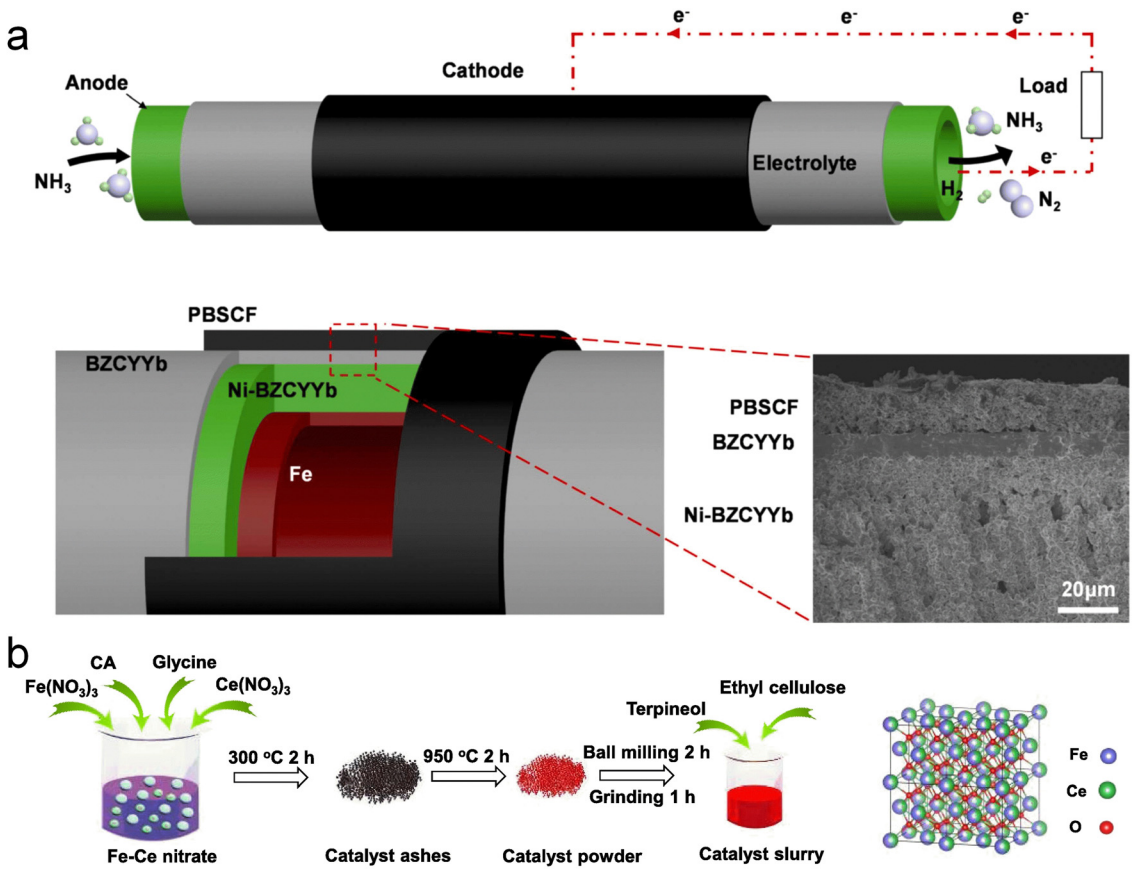

Fig. 16 (a) Schematic representation of a tubular cell utilizing NH_3 as the fuel.[173] (b) Schematic diagram of the synthesis process and the crystal structure of the Fe–CeO_x (Fe : Ce = 6 : 4) catalyst. Reproduced with permission.[175] Copyright 2022, Elsevier.

power generation. Although elevated temperatures facilitate NH_3 decomposition, they also increase energy consumption and system maintenance costs in DA-PCFCs. Furthermore, lower temperatures can result in incomplete NH_3 decomposition, leading to issues such as Ni nitridation in the Ni-based cermet anode and poor stability of DA-PCFCs. This necessitates the development of catalysts with enhanced NH_3 decomposition activity at lower temperatures. Fortunately, numerous catalysts have been developed in the field of NH_3 thermal decomposition, some of which demonstrate promising activity at lower temperatures and can be employed in external NH_3 cracking reactors for DA-PCFCs.[183,184] In particular, the unique structural and performance characteristics of high-entropy alloys (HEAs) have made them a focal point of research in catalysis. Recently, Wang *et al.* have demonstrated the potential of CoMoFeNiCu HEA for NH_3 decomposition.[84] While there have been limited reports on the application of high-entropy alloys as anodes or anode catalytic layers in DA-PCFCs, their potential in this field is promising. Furthermore, tailoring the catalyst morphology, particularly through the design of nanostructured catalysts or single-atom catalysts, enables complete NH_3 conversion at lower temperatures.[185,186] This may allow the electrochemical performance of DA-PCFCs to approach that of H_2-fueled PCFCs. Finally, DFT calculations can provide insights into the kinetics of NH_3 adsorption, the initial N–H bond cleavage, and N_2 desorption on the catalyst surface, thereby elucidating the rate-limiting step in the overall NH_3 decomposition process. This knowledge can guide the rational design and development of new catalytic materials that exhibit high activity for NH_3 decomposition at lower temperatures, enabling more efficient and sustainable processes.

5.2.2. Design of anode catalytic layer. Adding a catalytic layer with high NH_3 decomposition activity to the anode of DA-PCFCs can promote NH_3 decomposition, reduce direct contact between the anode and high-concentration NH_3, and thereby enhance the overall performance and stability of DA-PCFCs. Current reports on DA-PCFC anode catalytic layers consistently demonstrate performance improvements not only for DA-PCFCs but also for H_2 fueled PCFCs, suggesting that the catalyst layers may participate in the HOR on the anode side.[100,173–176] Consequently, in addition to seeking high NH_3 decomposition activity, it is crucial to consider the TEC matching and chemical compatibility between the catalyst layer material and the Ni-based cermet anode. Mismatched thermal expansion behavior can lead to delamination between the catalytic layer and anode during temperature cycling, severely impacting the electrochemical performance and stability of DA-PCFCs.

5.2.3. DA-PCFC stack design. Currently, research on DA-PCFCs is primarily focused on button cells, with no reports on

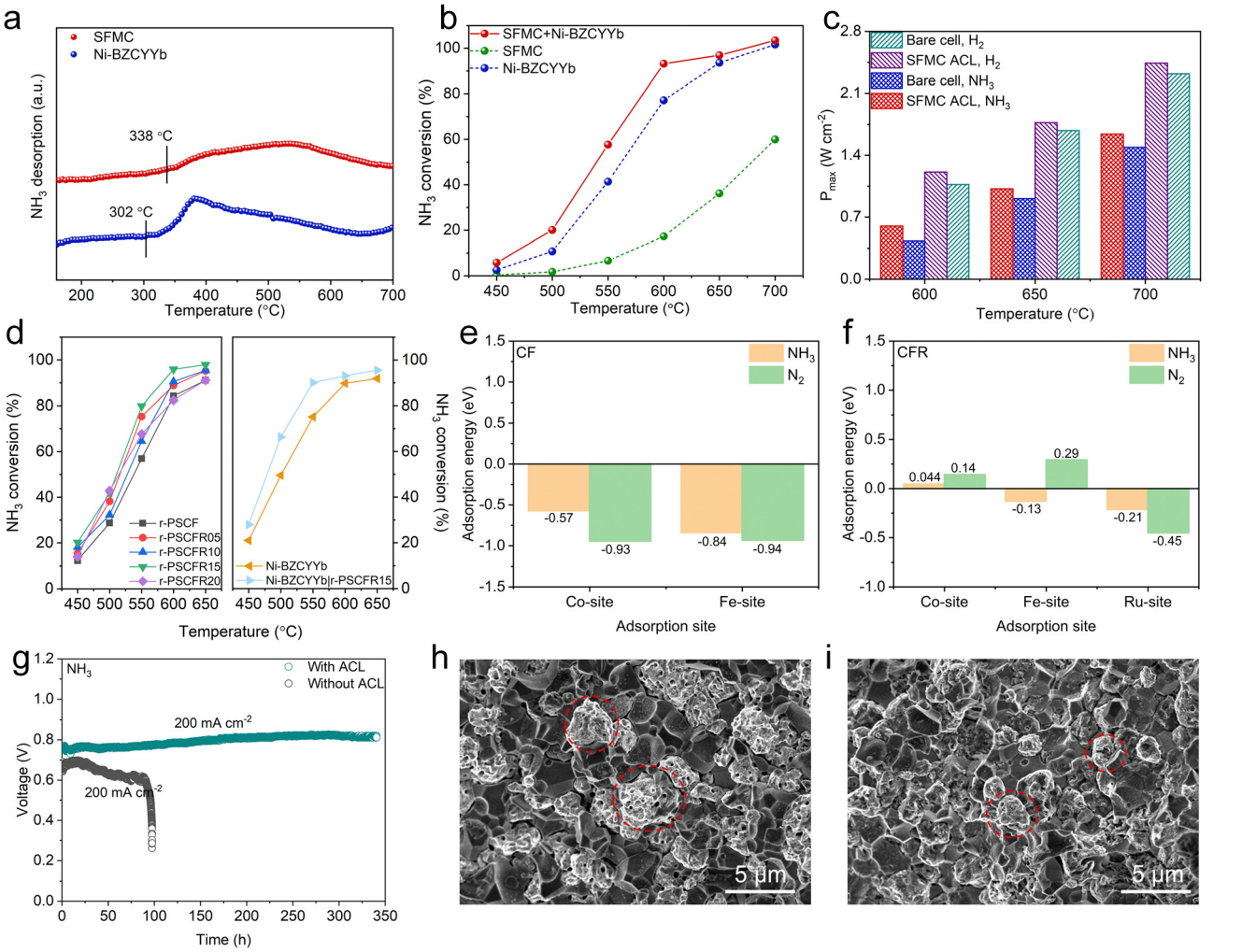

Fig. 17 (a) NH_3 temperature-programmed desorption profiles of r-SFMC and Ni–BZCYYb. (b) NH_3 catalytic activities of r-SFMC, Ni–BZCYYb, and their mixture. (c) PPDs of DA-PCFCs with and without r-SFMC ACL fueled by wet H_2 and dry NH_3. Reproduced with permission.[176] Copyright 2023, Wiley-VCH. (d) NH_3 decomposition rates of r-PSCF, r-PSCFR05, r-PSCFR10, r-PSCFR15, r-PSCFR20, Ni–BZCYYb, and Ni–BZCYYb|r-PSCFR15. E_{NH_3} and E_{N_2} calculated for (e) CF(011) and (f) CFR(011). (g) The operational stability of DA-PCFCs under NH_3 fuel conditions. The SEM images of Ni–BZCYYb anodes of DA-PCFCs (h) without ACL and (i) with r-PSCFR15 ACL after the stability test. Reproduced with permission.[100] Copyright 2024, Wiley-VCH.

kilowatt-level power output DA-PCFC stacks. Future research on DA-PCFCs should not only focus on developing anodes or catalysts with excellent NH_3 decomposition activity but also on the design, fabrication, and analysis of DA-PCFC stacks. In recent years, extensive research has been conducted on NH_3-fueled oxygen-ion conducting SOFCs (NH_3–O–SOFCs) and H_2-fueled PCFC stacks, which may provide valuable insights for the design of DA-PCFC stacks. Kishimoto *et al.* developed an NH_3–O–SOFC stack using 30 planar anode-supported cells, achieving a PPD of up to 1 kW and durability of 1000 h at 750 °C.[187] During the stack stability test, an energy conversion efficiency of 57% was attained at a PPD of 700 W. Song *et al.* proposed a two-step sintering method for fabricating large PCFC cells with excellent mechanical properties, optimizing the anode/electrolyte interface.[188] The stack using these large PCFC cells demonstrated stable operation for over 350 h at 600 °C. Furthermore, studies on modeling, thermodynamics, kinetics, and cost analysis of NH_3–O–SOFC and PCFC stacks can provide valuable guidance for DA-PCFC stack research. However, NH_3 can compromise pipeline integrity, causing embrittlement and corrosion that may lead to leaks. This also remains a critical area for future research.

6. Conclusions

PCCs represent a promising energy conversion technology, enabling both the storage of excessive renewable electricity *via* NH_3 synthesis and on-demand electricity generation from NH_3. This review comprehensively introduces the reaction mechanisms of electricity-to-NH_3 interconversion in PCCs, analyzes the challenges of this technology and summarizes the research advancements in this field. Moreover, this review emphasizes the need for researchers to explore not only novel

catalytic electrodes and electrolyte materials, but also to optimize operating conditions and identify active sites for the NRR and HER in order to achieve efficient NH_3 production in PCECs. For DA-PCFCs, the development of anode electrodes or anode catalytic layers with high catalytic activity for NH_3, as well as the fabrication of DA-PCFC stacks, should be the primary focus of future research. This review aims to encapsulate the progress in PCC-based electricity-to-NH_3 interconversion technology and provide insights for future research in this field.

Author contributions

Mingzhuang Liang: conceptualization, visualization, and writing – original draft. Jinwook Kim: investigation and writing – review & editing. Xiaomin Xu: writing – review & editing. Hainan Sun: writing – review & editing. Yufei Song: writing – review & editing. SungHyun Jeon: writing – review & editing. Tae Ho Shin: supervision and writing – review & editing. Zongping Shao: supervision and writing – review & editing. WooChul Jung: supervision, writing – review & editing, and project administration.

Data availability

The data supporting the findings of this study are available in the manuscript, and additional data are available from the corresponding author upon reasonable request.

Conflicts of interest

There are no conflicts to declare.

Acknowledgements

This work was supported by Ceramic Strategic Technology R&D program through the Korea Institute of Ceramic Engineering & Technology (KICET) (grant NTIS no. 240002182). This work was also supported by the National Research Foundation of Korea (NRF) grant funded by the Korea government (MSIT) (2021M3H4A3A02086497). We appreciate the support from Research Institute of Advanced Materials.

Notes and references

1 H. Ding, W. Wu, C. Jiang, Y. Ding, W. Bian, B. Hu, P. Singh, C. J. Orme, L. Wang, Y. Zhang and D. Ding, *Nat. Commun.*, 2020, **11**, 1907.
2 F. Zhu, Z. Du, K. Xu, F. He, Y. Xu, Y. Liao and Y. Chen, *Adv. Energy Mater.*, 2024, **14**, 2401048.
3 D. Kim, I. Jeong, S. Ahn, S. Oh, H. N. Im, H. Bae, S. J. Song, C. W. Lee, W. Jung and K. T. Lee, *Adv. Energy Mater.*, 2024, **14**, 2304059.
4 Y. Wang, Y. Ling, B. Wang, G. Zhai, G. Yang, Z. Shao, R. Xiao and T. Li, *Energy Environ. Sci.*, 2023, **16**, 5721–5770.
5 S. Choi, T. C. Davenport and S. M. Haile, *Energy Environ. Sci.*, 2019, **12**, 206–215.
6 J. H. Kim, J. Hong, D.-K. Lim, S. Ahn, J. Kim, J. K. Kim, D. Oh, S. Jeon, S.-J. Song and W. Jung, *Energy Environ. Sci.*, 2022, **15**, 1097–1105.
7 J. H. Kim, K. Jang, D.-K. Lim, S. Ahn, D. Oh, H. Kim, J. Seo, P.-P. Choi and W. Jung, *J. Mater. Chem. A*, 2022, **10**, 2496–2508.
8 F. Jiao and B. Xu, *Adv. Mater.*, 2019, **31**, 1805173.
9 N. Tsvetkov, D. Kim, I. Jeong, J. H. Kim, S. Ahn, K. T. Lee and W. Jung, *Adv. Mater. Technol.*, 2023, **8**, 2201075.
10 S. H. Oh, S.-Y. Park, S. Kim, K. J. Yoon, H. C. Shin, K. T. Lim and J.-H. Lee, *J. Korean Ceram. Soc.*, 2024, **61**, 34–43.
11 Z. Wan, Y. Tao, J. Shao, Y. Zhang and H. You, *Energy Convers. Manage.*, 2021, **228**, 113729.
12 A. Afif, N. Radenahmad, Q. Cheok, S. Shams, J. H. Kim and A. K. Azad, *Renewable Sustainable Energy Rev.*, 2016, **60**, 822–835.
13 D. S. Dhawale, G. Kaur and S. Giddey, *Inorg. Chem. Front.*, 2023, **10**, 6176–6192.
14 A. C. Chien, W. Y. Chen and M. S. Zheng, *J. Electrochem. Soc.*, 2023, **170**, 044505.
15 C. Smith, A. K. Hill and L. Torrente-Murciano, *Energy Environ. Sci.*, 2020, **13**, 331–344.
16 R. Li, T. Li, X. Liu, C. Xie, Q. Zhen, S. Bashir and J. L. Liu, *Energy Sci. Eng.*, 2023, **11**, 2293–2301.
17 R. K. Sharma, H. Patel, U. Mushtaq, V. Kyriakou, G. Zafeiropoulos, F. Peeters, S. Welzel, M. C. Van De Sanden and M. N. Tsampas, *ACS Energy Lett.*, 2020, **6**, 313–319.
18 Y.-i Kwon, S. K. Kim, Y. B. Kim, S. J. Son, G. D. Nam, H. J. Park, W.-C. Cho, H. C. Yoon and J. H. Joo, *ACS Energy Lett.*, 2021, **6**, 4165–4172.
19 I. Goyal, N. C. Kani, S. A. Olusegun, S. Chinnabattigalla, R. R. Bhawnani, K. D. Glusac, A. R. Singh, J. A. Gauthier and M. R. Singh, *ACS Energy Lett.*, 2024, **9**, 4188–4195.
20 T.-N. Ye, S.-W. Park, Y. Lu, J. Li, M. Sasase, M. Kitano and H. Hosono, *J. Am. Chem. Soc.*, 2020, **142**, 14374–14383.
21 H. M. Vieri, M.-C. Kim, A. Badakhsh and S. H. Choi, *Energies*, 2024, **17**, 441.
22 K. Wang, H. Chen, S.-D. Li and Z. Shao, *J. Mater. Chem. A*, 2022, **10**, 24813–24823.
23 J. Yu, L. Liu, Y. Du, Y. Li, D. Zhang, B. Li, X. Liu, L. Cheng, X. Zhang and Y. Zhang, *Energy Technol.*, 2024, **12**, 2401169.
24 B. Lee, D. Lim, H. Lee and H. Lim, *Renewable Sustainable Energy Rev.*, 2021, **143**, 110963.
25 E. D. Wachsman and K. T. Lee, *Science*, 2011, **334**, 935–939.
26 Y. Song, X. Zhang, K. Xie, G. Wang and X. Bao, *Adv. Mater.*, 2019, **31**, 1902033.
27 S. Park, E.-I. Kim, B. Singh and S.-J. Song, *J. Korean Ceram. Soc.*, 2024, **61**, 419–428.
28 C. Zhao, Y. Li, W. Zhang, Y. Zheng, X. Lou, B. Yu, J. Chen, Y. Chen, M. Liu and J. Wang, *Energy Environ. Sci.*, 2020, **13**, 53–85.
29 A. Hauch, R. Küngas, P. Blennow, A. B. Hansen, J. B. Hansen, B. V. Mathiesen and M. B. Mogensen, *Science*, 2020, **370**, eaba6118.

30 J.-h Myung, D. Neagu, D. N. Miller and J. T. Irvine, *Nature*, 2016, **537**, 528–531.
31 M. Liang, Y. Wang, Y. Song, D. Guan, J. Wu, P. Chen, A. Maradesa, M. Xu, G. Yang, W. Zhou, W. Wang, R. Ran, F. Ciucci and Z. Shao, *Appl. Catal., B*, 2023, **331**, 122682.
32 M. Liang, Y. Song, D. Liu, L. Xu, M. Xu, G. Yang, W. Wang, W. Zhou, R. Ran and Z. Shao, *Appl. Catal., B*, 2022, **318**, 121868.
33 Y. Song, J. Liu, Y. Wang, D. Guan, A. Seong, M. Liang, M. J. Robson, X. Xiong, Z. Zhang, G. Kim, Z. Shao and F. Ciucci, *Adv. Energy Mater.*, 2021, **11**, 2101899.
34 B. Wang, T. Li, F. Gong, M. H. D. Othman and R. Xiao, *Fuel Process. Technol.*, 2022, **235**, 107380.
35 F. Liu, D. Ding and C. Duan, *Adv. Sci.*, 2023, **10**, 2206478.
36 M. Ni, M. K. Leung and D. Y. Leung, *Int. J. Energy Res.*, 2009, **33**, 943–959.
37 Z. Li, C. Wang, I. T. Bello, M. Guo, N. Yu, M. Zhu and M. Ni, *J. Power Sources*, 2023, **556**, 232505.
38 M. Okazaki and J. Otomo, *Solid State Ionics*, 2024, **414**, 116649.
39 M. Okazaki and J. Otomo, *ACS Omega*, 2023, **8**, 40299–40308.
40 K. Miyazaki, H. Muroyama, T. Matsui and K. Eguchi, *Sustainable Energy Fuels*, 2020, **4**, 5238–5246.
41 Y. Han, W. Gao and Y. Qin, *Energy*, 2024, **297**, 131287.
42 Y. Du, X. Su, X. Wang, L. Ye and K. Xie, *New J. Chem.*, 2024, **48**, 10060–10066.
43 J. T. Irvine, S. Wilson, S. Amnuaypanich, G. J. Irvine, M. C. Verbraeken, K. Nowicki and G. M. Carins, *Faraday Discuss.*, 2023, **243**, 296–306.
44 S. Klinsrisuk and J. T. Irvine, *Catal. Today*, 2017, **286**, 41–50.
45 G. Weng, S. Lei, R. Wang, K. Ouyang, J. Dong, X. Lin, J. Xue, L.-X. Ding and H. Wang, *Joule*, 2023, **7**, 1333–1346.
46 H. Malerød-Fjeld, D. Clark, I. Yuste-Tirados, R. Zanón, D. Catalán-Martinez, D. Beeaff, S. H. Morejudo, P. K. Vestre, T. Norby, R. Haugsrud, J. M. Serra and C. Kjølseth, *Nat. Energy*, 2017, **2**, 923–931.
47 V. Kyriakou, I. Garagounis, E. Vasileiou, A. Vourros and M. Stoukides, *Catal. Today*, 2017, **286**, 2–13.
48 F. Liu, H. Deng, Z. Wang, A. M. Hussain, N. Dale, Y. Furuya, Y. Miura, Y. Fukuyama, H. Ding, B. Liu and C. Duan, *J. Am. Chem. Soc.*, 2024, **146**, 4704–4715.
49 K. Hong, M. Choi, Y. Bae, J. Min, J. Lee, D. Kim, S. Bang, H.-K. Lee, W. Lee and J. Hong, *Nat. Commun.*, 2023, **14**, 7485.
50 Y. Guo, S. Wang, R. Li, J. Yu, X. Zhang, M. Li, X. Zheng, J. Zhu, Y. Song, G. Wang and X. Bao, *Joule*, 2024, **8**, 2016–2032.
51 F. Kosaka, T. Nakamura, A. Oikawa and J. Otomo, *ACS Sustainable Chem. Eng.*, 2017, **5**, 10439–10446.
52 C.-Y. Yoo, J. H. Park, K. Kim, J.-I. Han, E.-Y. Jeong, C.-H. Jeong, H. C. Yoon and J.-N. Kim, *ACS Sustainable Chem. Eng.*, 2017, **5**, 7972–7978.
53 R. Lan, J. T. Irvine and S. Tao, *Sci. Rep.*, 2013, **3**, 1145.
54 Y. Zhou, E. Liu, Y. Chen, Y. Liu, L. Zhang, W. Zhang, Z. Luo, N. Kane, B. Zhao and L. Soule, *ACS Energy Lett.*, 2021, **6**, 1511–1520.
55 F. He, M. Hou, D. Liu, Y. Ding, K. Sasaki, Y. Choi, S. Guo, D. Han, Y. Liu, M. Liu and Y. Chen, *Energy Environ. Sci.*, 2024, **17**, 3898–3907.
56 C. Duan, R. Kee, H. Zhu, N. Sullivan, L. Zhu, L. Bian, D. Jennings and R. O'Hayre, *Nat. Energy*, 2019, **4**, 230–240.
57 M. A. Shipman and M. D. Symes, *Catal. Today*, 2017, **286**, 57–68.
58 S. Gunduz, D. J. Deka and U. S. Ozkan, *J. Catal.*, 2020, **387**, 207–216.
59 Q. Hu, C. Tian, D. Bao, H. Zhong and X. Zhang, *Next Energy*, 2024, **4**, 100144.
60 A. L. Garden and E. Skulason, *J. Phys. Chem. C*, 2015, **119**, 26554–26559.
61 E. Skulason, T. Bligaard, S. Gudmundsdóttir, F. Studt, J. Rossmeisl, F. Abild-Pedersen, T. Vegge, H. Jónsson and J. K. Nørskov, *Phys. Chem. Chem. Phys.*, 2012, **14**, 1235–1245.
62 J.-C. Liu, X.-L. Ma, Y. Li, Y.-G. Wang, H. Xiao and J. Li, *Nat. Commun.*, 2018, **9**, 1610.
63 A. U. Shetty and R. Sankannavar, *J. Energy Chem.*, 2024, **92**, 681–697.
64 W. Q. Li, M. Xu, J. S. Chen and T. N. Ye, *Adv. Mater.*, 2024, **36**, 2408434.
65 H. Kim, Y. S. Chung, T. Kim, H. Yoon, J. G. Sung, H. K. Jung, W. B. Kim, L. B. Sammes and J. S. Chung, *Solid State Ionics*, 2019, **339**, 115010.
66 J. Humphreys, R. Lan, D. Du, W. Xu and S. Tao, *Int. J. Hydrogen Energy*, 2018, **43**, 17726–17736.
67 W. Guo, Y. Li, S.-D. Li, Z. Shao and H. Chen, *Chem. Eng. J.*, 2024, **498**, 155124.
68 W. Guo, Y. Li, S.-D. Li, Z. Shao and H. Chen, *J. Mater. Chem. A*, 2024, **12**, 1200–1210.
69 K. Pei, Y. Zhou, K. Xu, H. Zhang, Y. Ding, B. Zhao, W. Yuan, K. Sasaki, Y. Choi, Y. Chen and M. Liu, *Nat. Commun.*, 2022, **13**, 2207.
70 Y. Huang, F. He, K. Xu, H. Gao, X. Zhang, Y. Xu, Z. Du, F. Zhu, W. Gong, C. Jian and Y. Chen, *Adv. Funct. Mater.*, 2024, **34**, 2409598.
71 Z. Liu, Z. Tang, Y. Song, G. Yang, W. Qian, M. Yang, Y. Zhu, R. Ran, W. Wang, W. Zhou and Z. Shao, *Nano-Micro Lett.*, 2022, **14**, 217.
72 H. Zhu, C. Karakaya and R. J. Kee, *Int. J. Green Energy*, 2022, **19**, 1568–1582.
73 M. M. Rahman, A. M. Abdalla, L. A. Omeiza, V. Raj, S. Afroze, M. S. Reza, M. R. Somalu and A. K. Azad, *Processes*, 2023, **11**, 2728.
74 M. Ni, D. Y. Leung and M. K. Leung, *J. Power Sources*, 2008, **183**, 687–692.
75 K. Xu, F. Zhu, M. Hou, C. Li, H. Zhang and Y. Chen, *Nano Res.*, 2023, **16**, 2454–2462.
76 S. Appari, V. M. Janardhanan, S. Jayanti, L. Maier, S. Tischer and O. Deutschmann, *Chem. Eng. Sci.*, 2011, **66**, 5184–5191.

77 Y. Song, H. Li, M. Xu, G. Yang, W. Wang, R. Ran, W. Zhou and Z. Shao, *Small*, 2020, **16**, 2001859.
78 S. Sorcar, H. Zinowits, E. P. Komarala, N. Moshe, I. Agranovich and B. A. Rosen, *J. Mater. Chem. A*, 2022, **10**, 24115–24126.
79 N. Khatun, C.-Y. Chiu, C.-J. Lin, J.-Y. Lin, S.-F. Wang and T. C.-K. Yang, *J. Power Sources*, 2024, **600**, 234252.
80 F. Zhong, X. Zhao, H. Fang, Y. Luo, S. Wang, C. Chen and L. Jiang, *Appl. Catal., B*, 2024, **360**, 124522.
81 X. Xiong, J. Yu, X. Huang, D. Zou, Y. Song, M. Xu, R. Ran, W. Wang, W. Zhou and Z. Shao, *J. Mater. Sci. Technol.*, 2022, **125**, 51–58.
82 Y. Yi, J. Chen, M. Xu, G. Yang, R. Ran, W. Zhou, W. Wang and Z. Shao, *Catalysts*, 2023, **13**, 996.
83 S. Mukherjee, S. V. Devaguptapu, A. Sviripa, C. R. Lund and G. Wu, *Appl. Catal., B*, 2018, **226**, 162–181.
84 P. Xie, Y. Yao, Z. Huang, Z. Liu, J. Zhang, T. Li, G. Wang, R. Shahbazian-Yassar, L. Hu and C. Wang, *Nat. Commun.*, 2019, **10**, 4011.
85 S. Sun, Q. Jiang, D. Zhao, T. Cao, H. Sha, C. Zhang, H. Song and Z. Da, *Renewable Sustainable Energy Rev.*, 2022, **169**, 112918.
86 B. Lu, L. Li, M. Ren, Y. Liu, Y. Zhang, X. Xu, X. Wang and H. Qiu, *Appl. Catal., B*, 2022, **314**, 121475.
87 A. Takahashi and T. Fujitani, *J. Chem. Eng. Jpn.*, 2016, **49**, 22–28.
88 C. A. Fernandez, N. M. Hortance, Y.-H. Liu, J. Lim, K. B. Hatzell and M. C. Hatzell, *J. Mater. Chem. A*, 2020, **8**, 15591–15606.
89 L. Hu, Z. Xing and X. Feng, *ACS Energy Lett.*, 2020, **5**, 430–436.
90 A. Skodra and M. Stoukides, *Solid State Ionics*, 2009, **180**, 1332–1336.
91 M. Ouzounidou, A. Skodra, C. Kokkofitis and M. Stoukides, *Solid State Ionics*, 2007, **178**, 153–159.
92 H. Shen, C. Choi, J. Masa, X. Li, J. Qiu, Y. Jung and Z. Sun, *Chem*, 2021, **7**, 1708–1754.
93 R. Zhao, H. Xie, L. Chang, X. Zhang, X. Zhu, X. Tong, T. Wang, Y. Luo, P. Wei and Z. Wang, *EnergyChem*, 2019, **1**, 100011.
94 S. H. Jeon, W. G. Jung, H. Bae, S. Ahn, B. Koo, W. J. Yu, S. Kim, D. H. Oh, U. Kim, S. A. Barnett, J. Seo, B.-J. Kim and W. C. Jung, *Adv. Mater.*, 2024, **36**, 2404103.
95 H. Zhang, K. Xu, F. He, Y. Zhou, K. Sasaki, B. Zhao, Y. Choi, M. Liu and Y. Chen, *Adv. Energy Mater.*, 2022, **12**, 2200761.
96 M. Choi, D. Kim, T. K. Lee, J. Lee, H. S. Yoo and W. Lee, *Adv. Energy Mater.*, 2025, **15**, 2400124.
97 C. Duan, J. Tong, M. Shang, S. Nikodemski, M. Sanders, S. Ricote, A. Almansoori and R. O'Hayre, *Science*, 2015, **349**, 1321–1326.
98 J. H. Kim, D. Kim, S. Ahn, K. J. Kim, S. Jeon, D.-K. Lim, J. K. Kim, U. Kim, H.-N. Im, B. Koo, K. T. Lee and W. C. Jung, *Energy Environ. Sci.*, 2023, **16**, 3803–3814.
99 H. Zhang, K. Xu, Y. Xu, F. He, F. Zhu, K. Sasaki, Y. Choi and Y. Chen, *Energy Environ. Sci.*, 2024, **17**, 3433–3442.
100 M. Liang, Y. Song, B. Xiong, D. Liu, D. Xue, L. Shen, K. Shi, Y. Song, J. Li, Q. Niu, M. G. Xu, F. Ciucci, W. Zhou and Z. Shao, *Adv. Funct. Mater.*, 2024, **34**, 2408756.
101 B. Stoeckl, V. Subotić, M. Preininger, M. Schwaiger, N. Evic, H. Schroettner and C. Hochenauer, *Electrochim. Acta*, 2019, **298**, 874–883.
102 J. Yang, A. F. S. Molouk, T. Okanishi, H. Muroyama, T. Matsui and K. Eguchi, *ACS Appl. Mater. Interfaces*, 2015, **7**, 28701–28707.
103 B. Miao, Z. Deng, P. Han, N. Yan, Z. Pan and S. H. Chan, *Chem. Eng. J.*, 2024, 159062.
104 N. Jantakananuruk, J. R. Page, C. D. Armstrong, J. Persky, R. Datta and A. R. Teixeira, *J. Power Sources*, 2022, **548**, 231999.
105 L. Chen, H. Zhang, K. Xu, Y. Xu, X. Zhang, F. Zhu, F. He and Y. Chen, *Mater. Today Catal.*, 2024, **7**, 100072.
106 H. Lan, J. Chu, X. Chen, Q. Zhou, W. Jin, Y. Zhang and J. Zhou, *J. Power Sources*, 2024, **593**, 233987.
107 Y. Wang, Y. Gu, H. Zhang, J. Yang, J. Wang, W. Guan, J. Chen, B. Chi, L. Jia, H. Muroyama, T. Matsui, K. Eguchi and Z. Zhong, *Appl. Energy*, 2020, **270**, 115185.
108 Y. Zhang, B. Chen, D. Guan, M. Xu, R. Ran, M. Ni, W. Zhou, R. O'Hayre and Z. Shao, *Nature*, 2021, **591**, 246–251.
109 J. Chen, W. Gao, L. Zhu, H. Tao, S. Feng, H. Cao, J. Guo, Y. Chen and P. Chen, *J. Mater. Chem. A*, 2024, **12**, 26667–26677.
110 M. Li, B. Hua, W. Wu, L.-C. Wang, Y. Ding, M. M. Welander, R. A. Walker and D. Ding, *Mater. Today*, 2022, **60**, 31–40.
111 L. Cheng, Y. Zhou, L. Luo, L. Wang, X. Xu, D. Guan, W.-H. Huang, C.-W. Pao, Z. Hu, J. Zhou, S. Wang and Z. Shao, *Chem. Eng. J.*, 2025, **505**, 159587.
112 S. Zhai, R. Zhao, H. Liao, L. Fu, S. Hao, J. Cai, Y. Wu, J. Wang, Y. Jiang, J. Xiao, T. Liu and H. Xie, *J. Energy Chem.*, 2024, **96**, 39–48.
113 L. Zhu, C. Cadigan, C. Duan, J. Huang, L. Bian, L. Le, C. H. Hernandez, V. Avance, R. O'Hayre and N. P. Sullivan, *Commun. Chem.*, 2021, **4**, 121.
114 G. Marnellos and M. Stoukides, *Science*, 1998, **282**, 98–100.
115 W. Wang, X. Cao, W. Gao, F. Zhang, H. Wang and G. Ma, *J. Membr. Sci.*, 2010, **360**, 397–403.
116 J. Otomo, N. Noda and F. Kosaka, *ECS Trans.*, 2015, **68**, 2663.
117 F. Kosaka, N. Noda, T. Nakamura and J. Otomo, *J. Mater. Sci.*, 2017, **52**, 2825–2835.
118 F. Kosaka, T. Nakamura and J. Otomo, *J. Electrochem. Soc.*, 2017, **164**, F1323.
119 Y. Kobayashi, N. Shimoda, Y. Kimura and S. Satokawa, *ECS Trans.*, 2017, **75**, 43.
120 M. Okazaki and J. Otomo, *ECS Trans.*, 2022, **109**, 3.
121 E. Vasileiou, V. Kyriakou, I. Garagounis, A. Vourros, A. Manerbino, W. Coors and M. Stoukides, *Solid State Ionics*, 2016, **288**, 357–362.
122 K. Wang, W. Zan, Y. Li, S. D. Li, Z. Shao and H. Chen, *Adv. Funct. Mater.*, 2024, 2418404.

123 E. Vasileiou, V. Kyriakou, I. Garagounis, A. Vourros and M. Stoukides, *Solid State Ionics*, 2015, **275**, 110–116.
124 Y. Guo, B. Liu, Q. Yang, C. Chen, W. Wang and G. Ma, *Electrochem. Commun.*, 2009, **11**, 153–156.
125 J. Yin, X. Wang, J. Xu, H. Wang, F. Zhang and G. Ma, *Solid State Ionics*, 2011, **185**, 6–10.
126 D. S. Yun, J. H. Joo, J. H. Yu, H. C. Yoon, J.-N. Kim and C.-Y. Yoo, *J. Power Sources*, 2015, **284**, 245–251.
127 C. Solís, L. Navarrete, M. Balaguer and J. M. Serra, *J. Power Sources*, 2014, **258**, 98–107.
128 C. Solis, L. Navarrete, S. Roitsch and J. M. Serra, *J. Mater. Chem.*, 2012, **22**, 16051–16059.
129 V. Kyriakou, I. Garagounis, A. Vourros, E. Vasileiou and M. Stoukides, *Joule*, 2020, **4**, 142–158.
130 H. Zhu, S. Ricote, C. Duan, R. P. O'Hayre and R. J. Kee, *J. Electrochem. Soc.*, 2018, **165**, F845.
131 J. Yang, T. Akagi, T. Okanishi, H. Muroyama, T. Matsui and K. Eguchi, *Fuel Cells*, 2015, **15**, 390–397.
132 M. Kishimoto, N. Furukawa, T. Kume, H. Iwai and H. Yoshida, *Int. J. Hydrogen Energy*, 2017, **42**, 2370–2380.
133 Y. Luo, Y. Shi, S. Liao, C. Chen, Y. Zhan, C.-T. Au and L. Jiang, *J. Power Sources*, 2019, **423**, 125–136.
134 J. Cao, Y. Ji and Z. Shao, *Energy Environ. Sci.*, 2022, **15**, 2200–2232.
135 Z. Liu, H. Di, D. Liu, G. Yang, Y. Zhu, Z. Luo, R. Ran, W. Wang, W. Zhou and Z. Shao, *Adv. Funct. Mater.*, 2024, 2420214.
136 S. Oh, M. J. Oh, J. Hong, K. J. Yoon, H.-I. Ji, J.-H. Lee, H. Kang, J.-W. Son and S. Yang, *iscience*, 2022, **25**, 105009.
137 G. Jeerh, M. Zhang and S. Tao, *J. Mater. Chem. A*, 2021, **9**, 727–752.
138 C. Chen, K. Wu, H. Ren, C. Zhou, Y. Luo, L. Lin, C. Au and L. Jiang, *Energy Fuels*, 2021, **35**, 11693–11706.
139 A. M. Mehdi, A. Hussain, M. Z. Khan, M. B. Hanif, R.-H. Song, W. W. Kazmi, M. M. Ali, S. Rauf, Y. Zhang and M. M. Baig, *Russ. Chem. Rev.*, 2023, **92**, RCR5098.
140 J. C. Ganley, F. Thomas, E. Seebauer and R. I. Masel, *Catal. Lett.*, 2004, **96**, 117–122.
141 H. Zhang, K. Xu, F. He, F. Zhu, Y. Zhou, W. Yuan, Y. Liu, M. Liu, Y. Choi and Y. Chen, *Adv. Mater.*, 2024, **36**, 2313966.
142 J. Yang, A. F. S. Molouk, T. Okanishi, H. Muroyama, T. Matsui and K. Eguchi, *ACS Appl. Mater. Interfaces*, 2015, **7**, 7406–7412.
143 A. Kruth and J. T. Irvine, *Solid State Ionics*, 2003, **162**, 83–91.
144 A. Kruth, R. Davies, M. Islam and J. T. S. Irvine, *Chem. Mater.*, 2007, **19**, 1239–1248.
145 K. Miyazaki, T. Okanishi, H. Muroyama, T. Matsui and K. Eguchi, *J. Power Sources*, 2017, **365**, 148–154.
146 J. Yun, G. Xiong, S. Kim, D. Bardgett, S. Choi and S. M. Haile, *ACS Energy Lett.*, 2024, **9**, 5520–5528.
147 O. B. Rizvandi, A. Nemati, M. Chen and H. L. Frandsen, *Int. J. Hydrogen Energy*, 2024, **50**, 961–976.
148 T. Su, B. Guan, J. Zhou, C. Zheng, J. Guo, J. Chen, Y. Zhang, Y. Yuan, W. Xie and N. Zhou, *Energy Fuels*, 2023, **37**, 8099–8127.
149 F. He, Q. Gao, Z. Liu, M. Yang, R. Ran, G. Yang, W. Wang, W. Zhou and Z. Shao, *Adv. Energy Mater.*, 2021, **11**, 2003916.
150 F. He, Z. Teng, G. Yang, C. Zhou, D. Guan, S. Chen, R. Ran, W. Wang, W. Zhou and Z. Shao, *J. Power Sources*, 2020, **460**, 228105.
151 Y. Song, J. Chen, M. Yang, M. Xu, D. Liu, M. Liang, Y. Wang, R. Ran, W. Wang, F. Ciucci and Z. Shao, *Small*, 2022, **18**, 2200450.
152 H. Zhang, Y. Zhou, K. Pei, Y. Pan, K. Xu, Y. Ding, B. Zhao, K. Sasaki, Y. Choi, Y. Chen and M. Liu, *Energy Environ. Sci.*, 2022, **15**, 287–295.
153 H. J. Jeong, W. Chang, B. G. Seo, Y. S. Choi, K. H. Kim, D. H. Kim and J. H. Shim, *Small*, 2023, **19**, 2208149.
154 Q. Ma, R. Peng, Y. Lin, J. Gao and G. Meng, *J. Power Sources*, 2006, **161**, 95–98.
155 L. Zhang and W. Yang, *J. Power Sources*, 2008, **179**, 92–95.
156 K. Xie, Q. Ma, B. Lin, Y. Jiang, J. Gao, X. Liu and G. Meng, *J. Power Sources*, 2007, **170**, 38–41.
157 N. Maffei, L. Pelletier, J. Charland and A. McFarlan, *J. Power Sources*, 2005, **140**, 264–267.
158 Y. Yoo, M. Tuck, N. Lim, A. McFarlan and N. Maffei, *ECS Trans.*, 2007, **7**, 2305.
159 Y. Aoki, S. Kobayashi, E. Tsuji and H. Habazaki, *ECS Trans.*, 2015, **68**, 2735.
160 K. Xie, R. Yan, G. Meng and X. Liu, *Ionics*, 2009, **15**, 115–119.
161 K. Xie, R. Yan, D. Dong, S. Wang, X. Chen, T. Jiang, B. Lin, M. Wei, X. Liu and G. Meng, *J. Power Sources*, 2008, **179**, 576–583.
162 Y. Yoo, N. Lim, M. Phongaksorn, A. McFarlan and N. Maffei, *ECS Trans.*, 2008, **12**, 691.
163 Y. Aoki, T. Yamaguchi, S. Kobayashi, C. Zhu and H. Habazaki, *ECS Trans.*, 2017, **78**, 1511.
164 Y. Aoki, T. Yamaguchi, S. Kobayashi, D. Kowalski, C. Zhu and H. Habazaki, *Glob. Chall.*, 2018, **2**, 1700088.
165 F. Liu, H. Deng, D. Diercks, P. Kumar, M. H. A. Jabbar, C. Gumeci, Y. Furuya, N. Dale, T. Oku, M. Usuda, P. Kazempoor, L. Fang, D. Chen, B. Liu and C. Duan, *Nat. Energy*, 2023, **8**, 1145–1157.
166 C. Zhou, J. Sunarso, J. Dai, R. Ran, Y. Song, F. He, W. Zhou and Z. Shao, *J. Membr. Sci.*, 2020, **596**, 117709.
167 R. Ren, Z. Wang, C. Xu, W. Sun, J. Qiao, D. W. Rooney and K. Sun, *J. Mater. Chem. A*, 2019, **7**, 18365–18372.
168 Y. Shin, Y.-d Kim, M. Sanders, S. P. Harvey, M. Walker and R. O'Hayre, *J. Mater. Chem. A*, 2022, **10**, 24839–24853.
169 M. Liang, F. He, C. Zhou, Y. Chen, R. Ran, G. Yang, W. Zhou and Z. Shao, *Chem. Eng. J.*, 2021, **420**, 127717.
170 H. Lee, H. Jung, C. Kim, S. Kim, I. Jang, H. Yoon, U. Paik and T. Song, *ACS Appl. Energy Mater.*, 2021, **4**, 11564–11573.
171 M. Liang, Y. Zhu, Y. Song, D. Guan, Z. Luo, G. Yang, S. P. Jiang, W. Zhou, R. Ran and Z. Shao, *Adv. Mater.*, 2022, **34**, 2106379.
172 Y. Song, Y. Chen, W. Wang, C. Zhou, Y. Zhong, G. Yang, W. Zhou, M. Liu and Z. Shao, *Joule*, 2019, **3**, 2842–2853.

173 Y. Pan, H. Zhang, K. Xu, Y. Zhou, B. Zhao, W. Yuan, K. Sasaki, Y. Choi, Y. Chen and M. Liu, *Appl. Catal., B*, 2022, **306**, 121071.
174 Z. Huang, T. Chen, X. Zhang, K. Liu, T. Li, S. Duo, H. Zhang, Y. Ling and S. Wang, *Ceram. Int.*, 2024, **50**, 10551–10559.
175 M. Hou, Y. Pan and Y. Chen, *Sep. Purif. Technol.*, 2022, **297**, 121483.
176 F. He, M. Hou, Z. Du, F. Zhu, X. Cao, Y. Ding, Y. Zhou, M. Liu and Y. Chen, *Adv. Mater.*, 2023, **35**, 2304957.
177 S. Wang, F. Gong, Q. Zhou, Y. Xie, H. Li, M. Li, E. Fu, P. Yang, Y. Jing and R. Xiao, *Appl. Catal., B*, 2023, **339**, 123134.
178 A. W. Tricker, K. L. Hebisch, M. Buchmann, Y.-H. Liu, M. Rose, E. Stavitski, A. J. Medford, M. C. Hatzell and C. Sievers, *ACS Energy Lett.*, 2020, **5**, 3362–3367.
179 S. Zhou, X. Yang, X. Xu, S. X. Dou, Y. Du and J. Zhao, *J. Am. Chem. Soc.*, 2019, **142**, 308–317.
180 V. C. Graça, L. I. Holz, A. J. Araújo, F. J. Loureiro and D. P. Fagg, *J. Energy Storage*, 2023, **68**, 107769.
181 I. Valov, B. Luerssen, E. Mutoro, L. Gregoratti, R. A. De Souza, T. Bredow, S. Günther, A. Barinov, P. Dudin, M. Martin and J. Janek, *Phys. Chem. Chem. Phys.*, 2011, **13**, 3394–3410.
182 D. Yao, C. Tang, L. Li, B. Xia, A. Vasileff, H. Jin, Y. Zhang and S. Z. Qiao, *Adv. Energy Mater.*, 2020, **10**, 2001289.
183 F. Chang, H. Wu, R. V. D. Pluijm, J. Guo, P. Ngene and P. E. De Jongh, *J. Phys. Chem. C*, 2019, **123**, 21487–21496.
184 K. Yamazaki, M. Matsumoto, M. Ishikawa and A. Sato, *Appl. Catal., B*, 2023, **325**, 122352.
185 K. Xu, Y. Y. Zhang, W. W. Wang, M. Peng, J. C. Liu, C. Ma, Y. W. Zhang, C. J. Jia, D. Ma and C. H. Yan, *Angew. Chem.*, 2025, **137**, e202416195.
186 Y. Li, Q. Guan, G. Huang, D. Yuan, F. Xie, K. Li, Z. Zhang, X. San and J. Ye, *Adv. Energy Mater.*, 2022, **12**, 2202459.
187 M. Kishimoto, H. Muroyama, S. Suzuki, M. Saito, T. Koide, Y. Takahashi, T. Horiuchi, H. Yamasaki, S. Matsumoto, H. Kubo, N. Takahashi, A. Okabe, S. Ueguchi, M. Jun, A. Tateno, T. Matsuo, T. Matsui, H. Iwai, H. Yoshida and K. Eguchi, *Fuel Cells*, 2020, **20**, 80–88.
188 S. Kim, H. Lee, C. Kim, I. Jang, K. Lee, S. Sun, D. Lee, J. Kim, K. Park, G. Lee, H. Jeong, H. Yoon, U. Paik and T. Song, *J. Power Sources*, 2022, **548**, 232082.

